THESIS FOR THE DEGREE OF DOCTOR OF PHILOSOPHY

Applying Microwave Technology in Short Range Radio Communication and Sensing Systems

Theory and Design

by

Emil Nilsson

Microtechnology and Nanoscience (MC2)
Chalmers University of Technology
SE-412 96 Göteborg, Sweden

School of Information Science, Computer and Electrical Engineering (IDE)
Halmstad University
Box 823
SE-301 18 Halmstad, Sweden

Göteborg, Sweden 2013

Applying Microwave Technology in Short Range Radio Communication and Sensing Systems - Theory and Design

ISBN 978-91-7385-914-1

Doktorsavhandlingar vid Chalmers tekniska högskola
Ny serie nr 3595
ISSN 0346-718X

Technical Report MC2-264
ISSN 1652-0769

Microwave Electronics Laboratory
Department of Microtechnology and Nanoscience - MC2
Chalmers University of Technology
SE-412 96 Göteborg, Sweden
Phone: +46 (0)31 772 1000

School of Information Science, Computer and Electrical Engineering (IDE)
Halmstad University
Box 823, SE-301 18 Halmstad, Sweden
Phone: +46 (0)35 16 7100

Cover illustration: *Short range communication and sensing*, by Elias Nilsson.

Printed by Chalmers Reproservice Göteborg, Sweden 2013

Abstract

Microwave technology continues to reach new areas and applications. Microwave based sensors create the possibility to sense objects in remote and hostile environments, while miniaturization makes the merge of radios, sensors, and computing into new small devices possible. Bridging the communication of the last 10 meters from numerous physical devices to a global network must be done wireless. Short range radio communication technology represents the most realistic untethered technology at hand.

Advanced digital control and processing electronics enable realization of sophisticated functionality and sophisticated communication protocols, also in low cost small size radio nodes. The high level of integration today common for digital electronics is increasingly utilized in analog electronics.

The need for small low power transceivers in many new applications is motivated by limited physical space and maintenance cost. The energy source for the device (usually a battery) sets the life time, the cost, and in some cases the physical dimensions of the final product. Low power electronics enable the use of more agile energy sources and longer lifetime with smaller batteries and energy harvesting techniques.

In this thesis a low power transceiver hardware and MAC protocol are proposed and investigated. A theory estimating noise in an envelope detector subject to a blocking signal is developed and used as a knowledge base for implementation of a Wake-up radio. The small Wake-up radio consumes 2.3μW and is designed in 130 nm CMOS using no other external components than the carrier substrate its mounted on. A survey of recently published low-power receivers is compared with estimation of lowest power consumption with optimized receiver topologies. Finally, the design of a low output-power radar interferometric sensor for industrial applications is presented together with measurements and simulations.

Acknowledgment

There are many people I wish to thank, who have supported me in my work. First I would like to mention Bertil Svensson, Urban Bilstrup, and Pelle Wiberg at Halmstad University for always being a great support, and of course all the people at MPE-lab. Thanks also go to my supervisor Peter Linnér, and to Lars Svensson at Chalmers for helpful technical discussions. Special thanks go to the people at ISY in Linköping who helped me with the CMOS implementations, Jonas Fritzin, Jacob Wikner, Atila Alvandpour, and many more. The single most important person for the finalization of this work has been Christer Svensson, thanks for all your ideas and help over time. Some special thanks and thoughts go to Johan Malm, who unfortunately has some rough times ahead. Johan has always been helpful, and open for a good technical debate. I wish you and your family the best. Finally I thank my family and friends for just being around and always up to new adventures.

List of publications

I. Emil Nilsson, Björn Nilsson, Lars Bengtsson, Bertil Svensson, Per-Arne Wiberg, and Urban Bilstrup, "A Low Power-Long Range Active RFID-system Consisting of Active RFID Backscatter Transponders", *IEEE International Conference on RFID-Technology and Applications 2010*, June 2010.

II. Emil Nilsson, Peter Linnér, Arne Sikö, Urban Bilstrup, and Per-Arne Wiberg, "A New CMOS Radio for Low Power RFID Applications", *IEEE International Conference on RFID-Technology and Applications 2010*, June 2010.

III. Emil Nilsson and Christer Svensson, "Envelope Detector Sensitivity and Blocking Characteristics", *20th European Conference on Circuit Theory and Design, ECCTD 2011*, Linköping, Sweden, August 28-31, 2011.

IV. Emil Nilsson and Christer Svensson, "Ultra Low Power Wake-up Radio using Envelope Detector and Transmission Line Voltage Transformer", *IEEE Journal on Emerging and Selected Topics in Circuits and Systems*, March 2013.

V. Emil Nilsson and Christer Svensson, "Power Consumption of Integrated Low-Power Receivers", *submitted for publication.*

List of publications from Licentiate thesis

VI. Emil Nilsson and Donald Malmberg, "Using microwave technology to create a topographical image of the burden surface in a blast furnace", *Proceedings of 5th Ironmaking Conference*, Buenos Aires, November 2005.

VII. Emil Nilsson and Lars Baath, "Radar Interferometric Measurements with a Planar Patch Antenna Array", *IEEE Sensors Journal*, pp. 1025-1031, July 2007.

VIII. Emil Nilsson and Donald Malmberg, "Using microwave interferometry to improve the blast furnace operation", *Scanmet III 3rd International Conference on Process Development in Iron and Steelmaking*, Luleå, Sweden, 8-11 June 2008.

Other publications

IX. Emil Nilsson and Martin Löfgren, "A GaAs MMIC Star Mixer for Ku-band Space Applications", *Swedish National Symposium GHz 2000*, March 2000.

X. Donald Malmberg, Pär Hahlin, and Emil Nilsson, "Microwave Technology in Steel and Metal Industry, an Overview", *ISIJ International*, Vol. 47, No. 4, pp. 533-538, 2007.

XI. Emil Nilsson, Björn Nilsson, and Eric Järpe, "A Pharmaceutical Anti-counterfeiting Method Using Time Controlled Numeric Tokens", *IEEE International Conference on RFID-Technology and Applications 2011*, September 2011.

XII. Emil Nilsson, Björn Nilsson, Urban Bilstrup, and Per-Arne Wiberg, "Ultra Low Power Radio for Pervasive Computing", *Embedded conference Scandinavia 2011*, October 2011.

XIII. Johansson Anders, Kubicka Jiri, Nilsson Emil, Wiebols Eric, Nilsson Anders, and Lindvall Martin, "An apparatus for detecting, measuring and selecting physiological signals and a method thereof", *Patent PCT 2002096287*, December 2002.

XIV. Emil Nilsson and Lars Baath, "Multi-dimensional imaging method and apparatus", *Patent US20070109177*, May 2007.

XV. Urban Bilstrup, Emil Nilsson, and Per-Arne Wiberg, "A device for wireless operation and method for operating the device", *Patent PCT 2008026988*, March 2008.

XVI. Urban Bilstrup, Emil Nilsson, and Per-Arne Wiberg, "Method and device for adjusting sensitivity", *Patent PCT 2009108106*, September 2009.

Preface

This thesis consist of two parts, one part about short range radio communication, and one part containing research on a interferometric sensor. Initially I started my research looking into sensors based on interaction between matter and electromagnetic waves using interferometric receiver and antenna array setups. I was mainly focusing on how to form a sensing beam, and how the signal should be processed to extract the intended information. The actual hardware was of limited interest, but had to deliver a decent signal. Important to consider was the noise contribution, and even more the phase stability; an interferometric system depend largely on information carried by the phase of the signal. The sensor system was intended for an interferometric topographical imaging system in a blast furnace and is covered by patent [1].

The reasons for not completing my PhD at this time were of both private and external origin; RWI, the company founded by my supervisor Lars Bååth, and where I pursued my research, moved its business to Lund. I could not accompany at this time since I was enjoying parental leave with two sweet toddlers.

During the work with the hardware platform enabling the interferometric measurements I developed an interest in the possibilities with integration of electronics, and especially analog high frequency electronics. Increased integration, as a mean for improved signal integrity and smaller form factor, highlighted the issue of power aware design of the sensor. By assigning a dedicated transceiver for each individual array antenna element a faster and more reliable imaging would be possible, but it would also increase the power density.

When scouting for new projects to continue my research I was asked to look into the design of low power radio electronics for RFID applications. This area combines analog electronics and high integration in a very challenging way. The reason for the emerging interest in this area was the ongoing development towards efficient short range radio communication solutions. Today this is part of a developing field, popularly termed Internet of Things (IoT), which actually includes areas such as RFID, Wireless Sensor Networks (WSN), Intelligent Transport Systems (ITS), and much more.

The development of RFID systems consider both hardware and medium access (MAC) protocols. In communication systems a better performance can be reached by co-design, or cross-layer design, of hardware and communication protocols. Our proposed system tried to make use of a very simplistic receiver, and a tailor made MAC protocol. Usually RFID nodes have a very limited power budget, and the reader has to do the major part of energy demanding processing. The number of applications possible to reach with the technology depend heavily on how much energy each node require and how much energy it

can store.

Common for many IoT applications, including RFID, is the need for an always aware radio receiver, a Wake-up Radio (WuR). The energy storage life time sets the system life time, maintenance cost, unit cost, and in some cases the size, of the final product. Development of low power electronics enables the use of smaller batteries, longer lifetime, or energy harvesting techniques to be used.

Thus, the work continued with focus on the Wake-up functionality. How to integrate and minimize the footprint of the receiver, and how to analyze and predict detector sensitivity in a modern radio environment with strong interference.

Contents

Acronyms and terms

ADC	Analog to Digital Converter.
A-RFID	Active-RFID.
ASIC	Application Specific Integrated Circuit.
ASK	Amplitude Shift Keying.
BAW	Bulk Acoustic Wave.
BER	Bit Error Rate.
BIST	Built In Self Test.
CLEAN	Numerical deconvolving process.
CMOS	Complementary Metal Oxide Semiconductor.
CW	Continuous Wave.
EM	Electromagnetic.
EPC	Electronic Product Code.
ESD	ElectroStatic Discharge.
FMCW	Frequency Modulated Continuous Wave.
FPGA	Field Programmable Gate Array.
FR4	Glass-reinforced epoxy laminate sheets.
FSK	Frequency Shift Keying.
ID	IDentity.
IF	Intermediate Frequency.
IoT	Internet of Things.
IP	Intellectual property.
IR	Infra Red.
ISM	Industrial, Scientific and Medical (radio bands).
ITS	Intelligent Transport System.
LNA	Low Noise Amplifier.
LO	Local Oscillator.
MAC	Medium Access Control.
MEFOS	Swedish metallurgical research institute.
MEM	Maximum Entropy Method.
MEMS	MicroElectroMechanical systems.
MIM	Metal Insulator Metal.
MOS	Metal Oxide Semiconductor.
MOST	MOS Transistor.
OOK	On-Off Keying.
PCB	Printed Circuit Board.
PLL	Phase Locked Loop.
PSF	Point Spread Function.
PSK	Phase Shift Keying.

Acronyms cont.

QAM	Quadrature Amplitude Modulation.
RCS	Radar Cross Section.
RF	Radio Frequency.
RFID	Radio Frequency IDentificaion.
SAR	Synthetic Aperture Radar.
SDR	Software Defined Radio.
SNR	Signal to Noise Ratio.
TRF	Tuned RF.
UWB	Ultra Wide Band.
VCO	Voltage Controlled Oscillator.
WLAN	Wireless LAN.
WSN	Wireless Sensor Network.
WuR	Wake-up Radio.

Chapter 1

Introduction

1.1 Motivation

Sensors embedded in networking and computing devices are predicted to generate a major part of the information carried over the internet in the near future. Already sometime between 2008 and 2009 there were more devices than people connected [2]. Miniaturization of computers, transceivers, and sensors continues and new services will be available. The evolution of an ubiquitous internet and global covering cellular network has called for new ways of looking at communication. Ad-hoc communications connect physical devices and sensors all around us with computing resources and networks around the world. However, a persisting hurdle for this vision of the Internet of Things (IoT) is the remaining 10 meters before reaching out to each device and object being sensed.

Short range low power microwave systems represent the only realistic technology to overcome this short but challenging distance, and thus such systems have to be utilized within new areas and applications; for communications purposes or as a part of sensor technologies.

1.2 Aim of this study

The aim of this study has been to address some important questions raised on the implementation of microwave electronics in short range radio communication and sensing.

How can we expand the utilization of microwave technology in communication and sensing? What limitations are imposed on technology from:

- environment
- market (cost)
- required coexistence with other systems

Are new ways in thinking of radio needed to reach otherwise inconceivable applications?

The research approach has been to develop new system solutions with real and commercial applications in mind. To understand and specify target performance, and interpret requirements into design parameters. To find limiting

factors for reaching successful implementation. To find, investigate, and improve some of the most important components of the system. Finally the ideas have been tested by simulation and implementation of real electronic systems.

1.3 Thesis contributions

- A proposed low-power transceiver architecture combined with a novel medium access protocol design.
- Implementation of low-frequency prototype of a low-power transceiver.
- Analytical expressions for impact of noise and blocker on the envelope detector.
- Monolithic implementation of ultra low-power high-frequency receiver.
- Measurement on integrated low-power envelope detector with blocking signal.
- System analysis of low power Wake-up Radios (WuR).
- Investigations on how 3D-imaging could improve a blast furnace operation.
- Development of 3D-imaging microwave interferometry system for industrial application.
- Measurements with 3D-imaging microwave interferometer.

1.4 Summary of appended papers

Paper I
"A Low Power-Long Range Active RFID-system Consisting of Active RFID Backscatter Transponders"

Summary

In this paper we present a novel active radio-frequency identification system consisting of transponders with low complexity, low power consumption, and long system-reading range. The transponder's low complexity and small circuit integration area indicate that the production cost is comparable to the one of a passive tag. The hardware keystone is the transponder's radio wake-up transceiver, which is a single oscillator with very low power consumption. The communication protocol, based on frequency signalling binary tree (see Sect. 2.2.1), contributes to the low complexity of the tag architecture. More than 1500 tags can be read per second. The average transponder ID read-out delay is 319 ms when there are 1000 transponders within reach of the interrogator. The calculated expected life time for a transponder is estimated to be almost three years.

Paper II
"A New CMOS Radio for Low Power RFID Applications"

Summary

A novel radio receiver circuit, functioning as a tuned active and detecting antenna, is described. The receiver is suggested to be part of a new radio system with the potential of competing with the range capability of active RFID-tags and, through its low power and long lifetime, with passive RFID-tags. The circuit is outlined and the functionality is verified by simulations and measurements. A 24 MHz discrete prototype showed better than -70 dBm sensitivity and 5 kHz bandwidth, with a power consumption of 102 μW. Simulations of a monolithic implementation were performed at 2.5 GHz. The detector is modelled by using 180 nm CMOS transistors. In simulations the power consumption for the detector is below 125 μW at a sensitivity of -83 dBm and a bandwidth of 9 MHz. Our conclusion is that this novel simple circuit architecture is well suited for monolithic implementation of a low power transceiver.

Paper III
"Envelope Detector Sensitivity and Blocking Characteristics"

Summary

This paper presents analytical expressions for the sensitivity of a low power envelope detector driven by a weak RF signal in the presence of a blocking signal. The envelope detector has been proposed for low power WuR's in applications such as RFID and wireless sensor systems. The theoretical results are verified with simulations of a modern short channel MOS transistor in a commonly used circuit topology. A discussion around a tutorial example of a radio frontend, consisting of an LNA and a detector, is presented. It is shown that the sensitivity of a low power envelope detector can reach -62 dBm with a low power LNA and in presence of a CW blocker.

Paper IV
"Ultra Low Power Wake-Up Radio using Envelope Detector and Transmission Line Voltage Transformer"

Summary

An ultra-low power wake-up radio receiver using no oscillators is described. The radio utilizes an envelope detector followed by a baseband amplifier and is fabricated in a 130nm CMOS process. The receiver is preceded by a passive RF voltage transformer, also providing 50 Ω antenna matching, fabricated as transmission lines on the FR4 chip carrier. A sensitivity of -47 dBm with 200 kbps OOK modulation is measured at a current consumption of 2.3 μA from a 1 V supply. No trimming is used. The receiver accepts a -13 dBm CW blocking signal, or modulated blockers 6 dB below the sensitivity limit, with no loss of sensitivity.

Paper V
"Power Consumption of Integrated Low-Power Receivers"

Summary

With the advent of Internet of Things (IoT) it has become obvious that RF designers have to be aware of power constraints, e.g. in the design of simplistic ultra-low power receivers acting as Wake-up radios (WuR). The objective of this work, one of the first systematic studies of power bounds for RF-systems, is to provide an overview and intuitive feel for how power consumption and sensitivity relate for WuRs. This was done by setting up circuit schematics for different radio receiver architectures to find analytical expressions for their output signal-to-noise ratio including power consumption, bandwidth, sensitivity, and carrier frequency. The result of the analytical expressions and optimizations of the circuits are energy per bit versus sensitivity, which are then compared with recent published low power receivers. The parameter set used in the analysis is meant to reflect typical values for integrated CMOS fabrication processes, and typical small sized RF lumped components.

Paper VI
"Using microwave technology to create a topographical image of the burden surface in a blast furnace"

Summary

In this paper a novel approach to use radar interferometry technology to create a 3D topographical image of the burden surface is described. By this approach the drawbacks of the presently used technologies used for burden surface determination are expected to be eliminated. MEFOS has tested an antenna unit that has the potential of measuring the full burden surface continuously during operation in the blast furnace and presents the result as a topographical image of the burden surface or a 3D image. Trials have so far been performed in laboratory as well as in a full scale charging model with promising result.

Paper VII
"Radar interferometric measurements with a planar patch antenna array"

Summary

A planar patch antenna array has been made for radar interferometry. The antenna array consists of 32 rectangular patches on a ceramic loaded teflon substrate. The patches are individually coupled to the microwave electronics in two orthogonal circular polarizations. The radar interferometer is intended for topographic imaging in industrial environment, in this case a blast furnace producing hot metal for the steel and metal industry. Ordinary imaging techniques with IR or visible radiation are not possible to use due to high temperatures and due to scattering from dust and particles. A model of a blast furnace burden material surface (see Fig.3.9) was measured and detected.

Paper VIII
"Using microwave interferometry to improve the blast furnace operation"

Summary

There are many known technologies that can be used to monitor surfaces, but most of them requires a transparent environment to be functional. In the blast furnace where the environment is full of dust and fume at high temperatures those technologies are not applicable. With a functional technology in such an environment the burden surface could be analyzed and monitored, which in its extension would lead to a way to control the charging operation in the blast furnace and thus a better use of raw material and also a better gas utilization. In this paper we will discuss the use of microwave technology as one technology with the potential to create a topographical image of the burden surface in the blast furnace during operation.

Chapter 2

Low power short range radio communication

Power has for a long time been the dominant design constraint for digital electronics. Among the motives we find the need to reduce cost for cooling and power, and the need for prolonged time between charges of mobile devices. In analog electronic design, and especially RF electronic design, the drive to reduce power has not been the same. Traditional RF electronic design has been more about getting better performance from given devices. However, along with the development of personal mobile communication also RF designers have become increasingly aware of the power issue. RF electronics have gradually become more integrated on ASIC devices together with the digital electronics, and thus are being subject to the same fabrication processes (mainly CMOS) and to the same scaling rules.

With the ongoing realization of the vision of Internet of Things (IoT), it has become even more obvious that RF designers have to be aware of the power constraint [3]. Sensors within the IoT have to survive on a single battery during their projected lifetime, or live on any available and harvested energy in its surroundings [4]. It would be virtually impossible to change batteries on each device in the considered swarm of connected items. For the most slimmed down sensors, communication has to be provided solitary by WuRs or similar simplistic radios. The communication distance is often short and require low power solutions, often referred to as short range devices.

There is no clear definition of what short range radio communication is, but a common view seems to be radio communication over a shorter range than 10 meters. New functionalities and applications may be reached if we can overcome these last 10 meters without wires, using low power wireless devices. From the ETSI homepage [www.etsi.org] we find the following description of what "Short Range Device" might include:

> "Short Range Devices (SRD) are radio devices that offer a low risk of interference with other radio services, usually because their transmitted power, and hence their range, is low. The definition 'Short Range Device' may be applied to many different types of wireless equipment, including various forms of:

- Access control (including door and gate openers)
- Alarms and movement detectors
- Closed-circuit television (CCTV)
- Cordless audio devices, including wireless microphones
- Industrial control
- Local Area Networks
- Medical implants
- UWB Sensors and Radars (such as ground probing radar)
- Remote control
- Radio frequency identification (RFID)
- Road Transport Telematics
- Telemetry

> Short range devices often benefit from a relaxed regulatory regime compared with other radio communications equipment. As general principle, a user is licence free to operate such equipment, some specific cases may require an individual licence."

The importance of the power issue for short range radio communication is underlined by the following citations.

– In the annual report 2012 of Berkeley Wireless Research Center it is written:

> "Wireless systems are evolving to a three tiered environment with a ubiquitous, embedded and transparent sensory swarm at the outer layer. Ultra-low-power realizations of integrated wireless sensor nodes are an essential condition for the swarm concept to become truly successful."

– According to a an article in EETIMES, Nordic Semiconductor's CEO, Svenn-Tore Larsen, said:

> "Once designers have an inexpensive way to add an interoperable wireless link to anything that's battery powered, even devices with the smallest batteries, the application potential is vast. Designers will come up with thousands of ways to use that link."

Research should aim at lowering the threshold for adding the wireless link. This can be accomplished by reducing the footprint, merging to commercially feasible technology bases, and not least, by reducing the power consumption. Parameters like linearity and sensitivity has often been prioritized over power consumption in wireless system work. More energy efficient hardware has reduced the energy demand, but system design has not been focusing on reaching least possible overall power consumption. This has changed and today power consumption is in focus from components through all system levels in radio engineering.

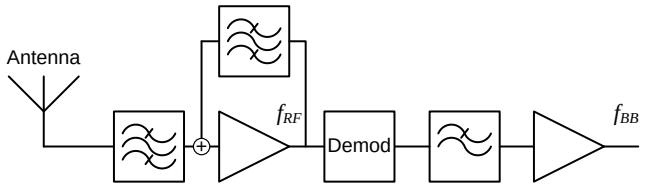

Figure 2.1: *Regenerative receiver. The positive feedback loop improves the gain of the pre-amplifier. The feedback is kept below the level feeding a self oscillation.*

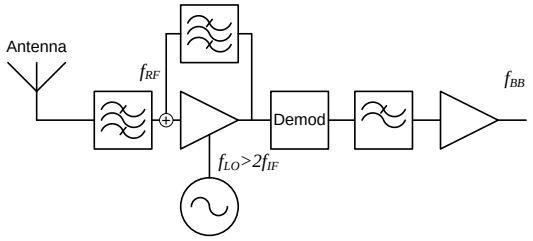

Figure 2.2: *Superregenerative receiver with a quench (sampling) oscillator. The positive feedback is periodically adjusted by the quench oscillator from a low level up to a level sustaining self-oscillation in the loop.*

2.1 Background

2.1.1 Receivers for low power applications

The set of available low power receiver architectures is rather limited. Low power radio solutions often use simple modulation schemes like ASK or FSK, with some exceptions such as the injection locked PSK receiver described in [5].

During the highly innovative radio era of the early 1900's, topologies such as the regenerative receiver, Fig. 2.1, and the super-regenerative receiver, Fig. 2.2, were invented. The regenerative and super-regenerative receivers use feedback to get the most out of poor amplifiers and devices. The positive loop gain of the regenerative receiver is kept below the level allowing self oscillation to build up ("the same signal is amplified many times"). This way gain is increased and selectivity is improved at the same time. While for the super-regenerative receiver the loop gain is repeatedly adjusted to allow self-oscillation to build up [6]. The loop gain is here controlled by the quench oscillator. The received signal is sampled at the quench frequency, and the oscillation builds up faster for stronger signal levels. Actually the regenerative receiver may also be used in a self-oscillation mode, for reception of CW signals (morse code). The feedback loop works both as an amplifier and as a heterodyne oscillator in this mode (oscillation frequency is set slightly offset to the CW frequency).

The promising properties of the regeneration phenomenon makes the regenerative and super-regenerative receivers candidates for low power radio. However, problems with stability and control seem to have prevented them from making true success.

The Tuned RF receiver (TRF) (also this is a revoked design from early radio), see Fig. 2.3, is basically a crystal radio and uses no oscillators. The

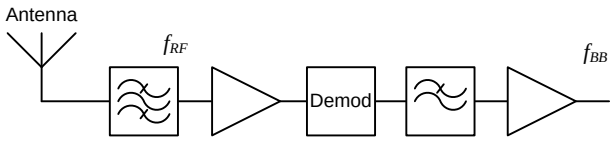

Figure 2.3: *Tuned RF receiver, TRF.*

TRF consists of an RF-filter and a pre-amplifier together with an envelope detector. A transformer may give passive voltage gain and provides some RF-filtering before the detector. This passive gain is no real power gain but only trades current for voltage by increasing the impedance level. If we want to use a common CMOS process for implementation, the energy detector can be designed with MOS transistors as the rectifying components. The envelope detector efficiency strongly depends on the RF carrier amplitude V_{RF}. The output baseband voltage is $V_O = kV_{RF}^2$, where k is a coefficient depending on technology and efficiency. Better sensitivity is reached by reducing bandwidth of the baseband filter, and thereby reducing channel capacity. The selectivity is solely depending on the RF-filter, and is rather poor.

It is worth noting that alos the superheterodyne is a candidate for low power radio, although hampered by having an always running local oscillator (LO) draining energy. The superheterodyne will be further treated in the thesis in section 2.1.2 and section 2.4.1.

2.1.2 Related work

The Berkeley PicoRadio project [7] has worked on ad-hoc sensor nodes and their system level requirements. They have identified the radio communication data link as one of the most challenging parts of these systems. According to Berkeley each node has to: use very small amounts of power to enable the use of energy scavenging ($<100\mu$W), have a low cost implementation ($<$1\$US), and have a small form factor ($<$cm^{-3}). That is for a complete sensor node, if it should be used ubiquitously. The small form factor imposes severe limitations on the antenna efficiency, and research work on solutions better exploiting the available volume of each node [8]. Further, wireless sensor nodes are required to function in a multitude of environments, embedded in or in close proximity to a large variation of materials such as metal, human tissue, air, etc. This requires different types of antennas and/or adaptive matching as in [9] and [10].

A survey of recent published low power receivers is found in, Fig. 2.4, where the consumed energy to receive a single bit is plotted as a function of the receiver sensitivity. The sensitivity is defined as the RF power needed to reach a raw bit error rate of BER=10^{-3}, before redundant coding and error corrections. The published receivers are used in applications ranging from general use in WSN to more spectacular use such as the heavy duty cycled receiver for e.g. insect flight control in [11]. Passive RFID nodes have inherently low sensitivity, since they are supplied by the incoming RF-energy being scavenged [12][13]. The passive transceivers using load-modulation have the drawback that they need to be optimized both for sensitivity to and rectification of the incoming radio energy. In [14] a passive "frequency conversion" data transmission method is

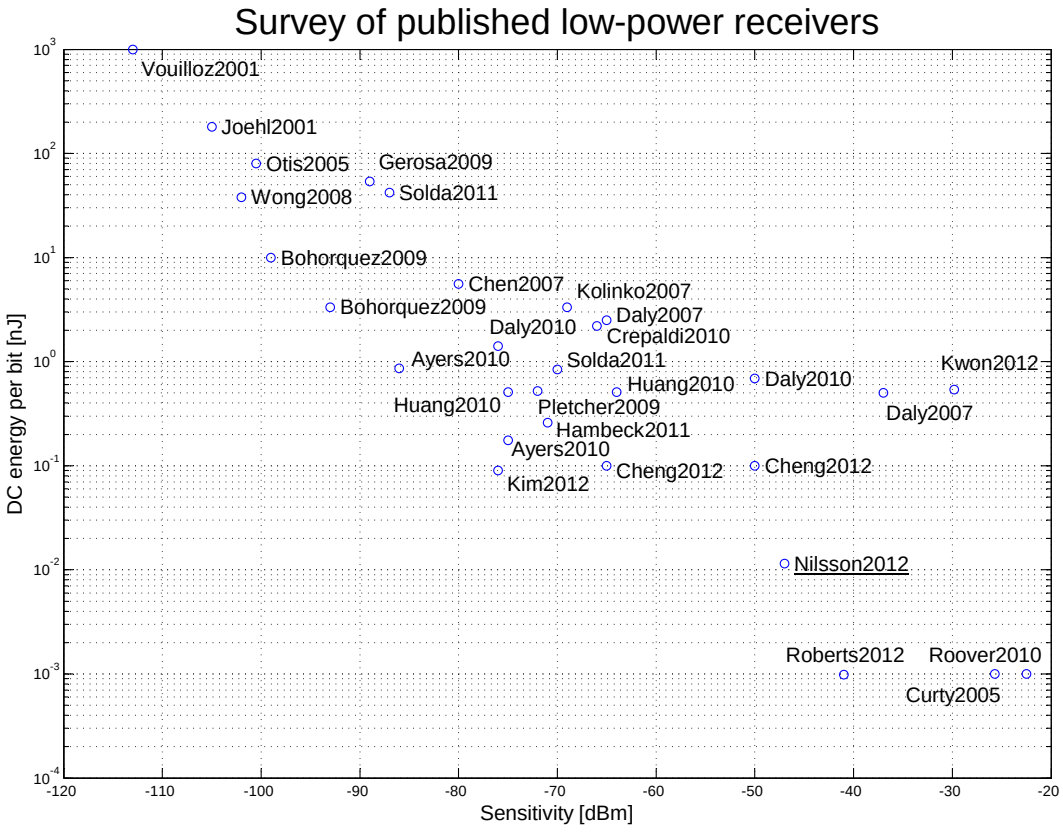

Figure 2.4: *Recent published low-power receivers. The DC power consumption to receive one bit is plotted against the receiver sensitivity.*

described as a way to circumvent this and to increase the reading range for medical implants.

Other ways of thinking in receiver design have been proposed. One example is the injection locked low power RC-oscillator in [5], where the radio channel efficiency is improved by using phase shift modulation rather than ASK or FSK. This is enabled by the synchronization of the oscillator phase with the received signal through the injection locking mechanism. Another example is the relaxed LO requirements presented in [15], where a resulting uncertain intermediate frequency (IF) is amplified and envelope detected. Yet another idea is to share the bias current to minimize power consumption, and "re-use" it in the LNA, mixer, and VCO. Examples of different techniques for this are found in [16] and [17].

Efficient, small size, and low cost resonant networks and reactive loads are needed in the design of oscillators, filters, transformers, and RF amplifiers. On-chip inductors are lossy and consume expensive silicon area, while off-chip components add to the component count and use the limited pad area for terminals. The on-chip losses can be compensated by amplifiers or active components in feedback loops, like regenerative receivers, but at the cost of DC-power. Further, the achievable Q for such setups is limited by sensitivity to temperature and process variations [18]. Microelectromechanical system (MEMS) components is a solution that have been proposed [19], but such components need to be placed off-chip with current CMOS technology. The use of the bond wires as inductors solves part of the problem [20]. On-chip tuning electronics is needed to mitigate the parameter spread in fabrication for both solutions. In summary, the question whether using on-chip or off-chip component involves a complicated cost/performance trade-off [21][22].

Beside physical building blocks and devices, a communication channel relies on a Medium Access (MAC) protocol controlling and scheduling the communication. Here duty cycling is a simple way to reduce average power consumption of the receiver, but at the cost of added latency and a requirement for good synchronization. Another approach to reduce power consumption is to minimize the functionality during the idle periods; meaning that high data rates are transferred with more power hungry radios using complex modulation, while simplistic ultra low power receivers function as WuRs during idle time. Receiver and transmitter topology is determined by the modulation and MAC protocol being used. Such system consideration are covered for instance in [23] [24][25][26].

Specifically designed MAC protocols could enable very simple transceivers/transponders to be used. Eliminating the always running clock used for duty-cycled wake-up of the transponder would save power, but would require an asynchronous wake-up functionality to be introduced. More over, if the LO could be removed from the transceiver/transponder the power consumption may be reduced considerably.

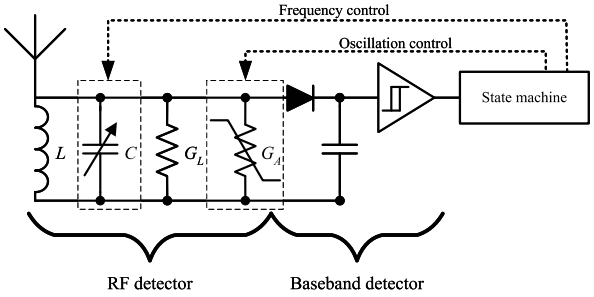

Figure 2.5: *Principle configuration of bi-stable wake-up radio transponder architecture.*

2.2 A low power RFID-system with a specifically designed MAC protocol

The principles for passive RFID were invented along with radar during World War II [27][28]. By actively changing the backscatter properties of an object a modulated signal is retransmitted to a radiating RFID reader, and the identity of the object can be decoded from the reflected signal.

RFID systems are often classified as either being passive or active. The passive RFID rely on energy transmitted from the RFID-reader to power up the transponders. Radio energy is collected by a rectifier and stored in a capacitor. When enough energy is stored the electronics is started and the antenna reflection coefficient is modulated, e.g by switching the antenna load impedance. Active RFID depends on other energy supplies and may use other modulations techniques. Active RFID (A-RFID) transponders listen continuously or may save energy by being synchronized to the RFID-reader and listen periodically for interrogation signals. The life time for the energy source of the active transponder is affected by how synchronization is performed, and various solutions for wake-up radios have been published.

Typical issues with RFID systems are low receiving sensitivity resulting in short reading range, awakening due to false signaling, and a need for cyclic synchronizing. RFID applications usually have asymmetric requirements on power consumption regarding the central reader and the distributed transponders, which can be used to minimize complexity in transponders by redistributing functionality to the reader.

An RFID system built on a frequency binary tree search protocol could use a very low complexity transponder with a resonant circuit changing from a low power, stable non-oscillating state to a second state of self-oscillation by excitation from an aerial radio pulse. This would eliminate the need for a complex communication protocol with synchronization. The transponder could consist of a single LC-oscillator operated in subthreshold region and thus exhibiting very low power consumption.

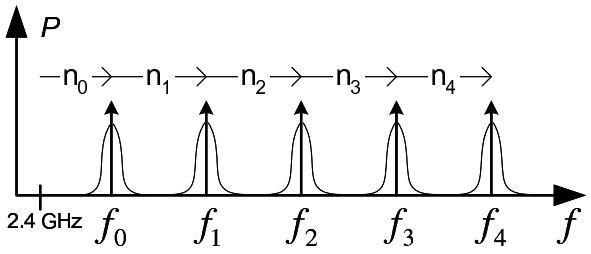

Figure 2.6: *Frequency spectrum allocation used by the communication protocol.*

2.2.1 Principle of operation

In this RFID system an LC-oscillator, see Figure 2.5, is used in the transponder as a wake-up radio. The oscillator is designed to consume low power by operating in the weak inversion region (subthreshold). The oscillator is biased near oscillation and a radio signal received by the antenna pushes the bias point into a region where stable oscillation is obtained, resulting in a signal being transmitted back (backscattered) to the reader on the same frequency. These are the two intended states of operation for the receiver, the idle state, where the receiver is armed and waiting for an input signal, and the active state, in which it has received an input signal and therefore is oscillating. The idle state corresponds to a bias point with lower loop gain, and the active state corresponds to a bias point with higher loop gain. The nonlinear response is essential for the ability to achieve stability in each of the described states. The necessary energy in the incoming pulse that may change state of the receiver depends on the nonlinearity of the active device, as well as on the Q-value of the tank circuit.

The protocol for communication between the transponder and reader is described in [29] and is of the binary tree type, meaning that the ID is extracted bit by bit when traversing a binary tree detecting whether the transponder's next ID-bit is a '0' or a '1'.

To extract bits in the transponder ID, the protocol uses frequency signaling. The transponders in the vicinity of the reader are first awakened by a beacon signal. The awakened transponders IDs are extracted by using four different frequencies, where every frequency corresponds to a two-bit combination in the ID as follows and is spread in the 2.45 GHz ISM band, see Figure 2.6.

f_0: is the beacon signal, 2400+n_0 [MHz], used to wake up all transponders within the reader's range

f_1: '00_{msb}', 2400+n_0+n_1 [MHz]

f_2: '10_{msb}', 2400+n_0+n_1+n_2 [MHz]

f_3: '01_{msb}', 2400+n_0+n_1+n_2+n_3 [MHz]

f_4: '11_{msb}', 2400+n_0+n_1+n_2+n_3+n_4 [MHz]

It is possible to identify all transponders in range for the reader without knowing anything in advance of the transponder population. The ID extraction

Table 2.1: System components data used for evaluation of communication protocol.

Transponder power consumption, idle state [mW]	0.02
Tag power consumption, active state [mW]	1.4
Tag sensitivity [dBm]	-72
Tag output power [dBm]	-10
Tag idle to active state [μs]	1.0
Reader sensitivity [dBm]	-85
Reader output power [dBm]	20

starts when the reader transmits the beacon signal (on frequency, f_0), awakening all transponders in reach. In the next step the reader transmits on all four frequencies, f_1–f_4, simultaneously. A transponder is initially "tuned" to the frequency corresponding to its two least significant ID bits, and the transponder transmits back, only, when receiving a signal at its "tuned" frequency. This method is iterated, traversing bit by bit, halving the transponder population. When the last bits are read one branch is finished, and next may be followed.

In some applications it is known which transponders that should be in vicinity of the reader. Instead of trying to read all transponders it is possible to selectively read transponders. If the ID of a transponder is already known by the reader, then it is possible to address that specific transponder. The reader uses the frequency "trail", which is composed of the bit combination in the transponder ID in a straightforward way. The addressing method is useful for saving transponder energy, only doing a minimal number of activations of the transponders.

2.2.2 Results and discussion

The proposed low power detector is listening without a running LO. It is in constant operation without duty cycling, thus enabling a short response time. However, the sensitivity to biasing conditions is clear in both measurements and simulations. Measurements on a low frequency prototype show that the circuit is fairly stable over time with a slight drift in the tens of millivolts range for the bias voltage keeping the circuit in idle state. A basic detector model predicts the sensitivity bandwidth to be controlled by the bias of the active elements, which is also confirmed by measurements.

False triggering may drain the power supply and must be minimized. Apart from using calibration strategies, this should also be handled at the higher protocol level. As an example, frequency hopping technique will be used, where each hop has the potential to trigger the receiver oscillations [29]. It follows that it is important to minimize the number of frequency hops used for addressing each single transponder.

The results from the simulations are presented as 1) read-out delay, the time it takes in average to read a transponder ID, and 2) the tag life time when draining the tag battery. Calculations are based on numbers in Table 2.1. All simulations have been made with the detector biased 1 mV below the level where the self induced oscillation starts.

The calculated expected life time of how many days a battery will last if the

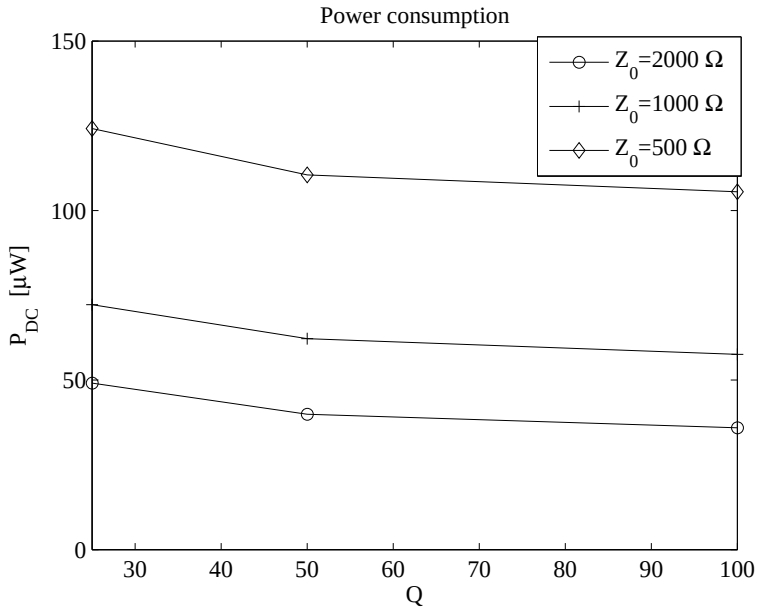

Figure 2.7: *Simulated power consumption for the wake-up transponder depicted in Fig. 2.5 in its idle state for different inductor Q-values and interfacing RF-port impedances (Z_0). With inductance $L = 5.216$ nH, transistor width W=175 µm (making up G_A), and at f_c=2.5 GHz.*

reader tries to read the transponders every 60 seconds is more than 900 days. The maximum throughput is 1570 transponders per second.

More than 1500 transponders can be read per second with the system. The average delay when reading a transponder ID in a population of 1000 transponders is 319 ms.

The theoretical reading range in free space is 50 meters. The estimated life time for a transponder, in this active RFID system, powered by a low-cost 7x7 square centimeter printed battery is almost three years. This is in a scenario where the transponder's ID is read out as often as 60 times per hour and only considering the energy content in the battery.

A matter of importance is the difference between final oscillation and the sensitivity center frequency of the detector. This will have an impact on how the detector may be used. If we want the detector to work as a backscatterer this difference must be incorporated in the communication protocol, otherwise the oscillation frequency has to be tuned during the transmitting period. In any case the current through the detector will increase and the incoming signal is detected.

The power consumption is as expected lowest for the implementation with a combination of high impedance and high Q-value. Further, the lowest current and power is found with the largest inductor, which in turn results in the smallest transistor. The variation in power consumption is seen in Fig. 2.7.

Wake-up radios not being based on duty cycling make each transponder reachable by the RFID reader at any time and do not need any advanced

synchronized wake-up algorithms. Reducing complexity of transponders infers a corresponding increase in reader complexity. The low complexity and low power consumption of the described backscatter radio transceiver enable low-cost transponders with long reading range and two-way communication between transponder and reader.

The principle of the transponder operation was proven with a discrete low frequency prototype. The discrete implementation may be transferred to a monolithic design performing at higher frequencies. Simulations of a monolithic implementation using 180 nm CMOS transistors were performed at 2.5 GHz. In simulations the power consumption for the detector is below 125 μW at a sensitivity of -83 dBm and a bandwidth of 9 MHz.

However, the simple analog hardware solution come at the cost of need for calibration to keep the transceiver in its stable state. Keeping the conductance $G = G_L - G_A$ as stable as possible is essential for the system. The important parameter here is the active device transconductance which is controlled by the bias current. The transconductance of a MOS device biased in the subthreshold region has an exponential temperature dependence. Several strategies are possible, one suggestion being self calibration with the potential to mitigate both fabrication and temperature variations. The calibration may be performed as a binary process homing in on the bias point just below noise induced self oscillation, a similar method is described in [30].

A more robust solution would be preferable, and given the complications associated with the bistable transceiver it is plausible to compare the bistable transceiver with a oscillator-free TRF receiver. The TRF receiver may initialize any transmitter on wake-up and thus form a complete transceiver if needed. An important argument for looking into the TRF receiver is that it is well suited for implementation in an ordinary CMOS process.

2.3 A low power oscillator-free CMOS TRF receiver

A TRF receiver performs envelope detection at the carrier frequency without any prior frequency conversion. Thus energy consuming oscillators and mixers are avoided, but at the cost of sensitivity and selectivity. In the TRF receiver selectivity is achieved by a preceding RF-filter. The receiver presented below is a TRF receiver without oscillators, neither in the RF chain nor in the baseband stages. No external components are used, except for a transmission line voltage transformer on the FR4 laminate carrying the RF-ASIC.

2.3.1 Description of the receiver architecture

A Wake-up radio has the single purpose to recognize a predetermined ID-code bit pattern in the air, and the chosen architecture is focused on simplicity. It uses no superregenerative solutions or oscillators, and no control or calibration loops such as phase locked loops. This enables a short startup time and avoid any lock-in processes adding to overall power consumption [13].

As much as possible of the radio functionality should be handled over to the interrogator or reader (the term "reader" emanates from the RFID community and is a bit misleading here since we only use downlink communication). A very

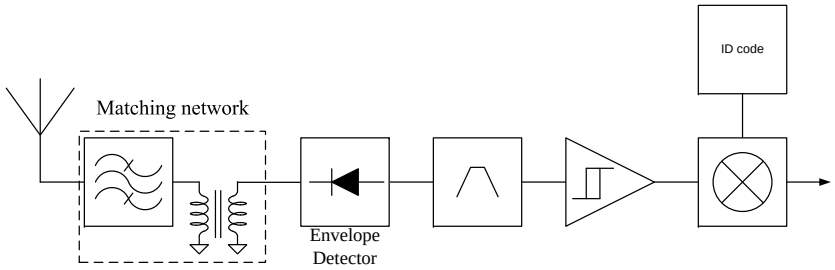

Figure 2.8: *Block diagram of low-power oscillator-free CMOS TRF receiver.*

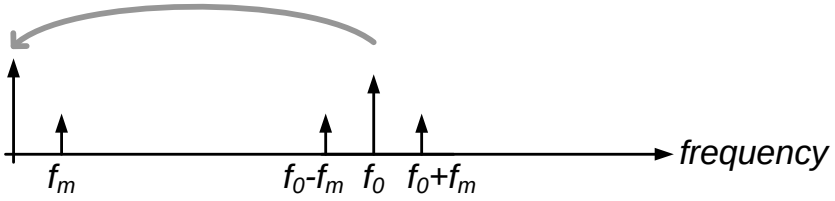

Figure 2.9: *Frequency translation by envelope detection of an ASK-modulated signal.*

limited amount of data will be sent at each wake up session, only a few hundred bits containing an ID-code. We use OOK modulation of the carrier; although this is spectral inefficient it is motivated by the short transmission bursts and the simplification of the receiver design. A carrier frequency of 2450 MHz (ISM) offers a good compromise between size and range, and an ability to see "around" corners and obstacles. The overall receiver block diagram is found in Fig.2.8.

Envelope detector

The incoming RF carrier drives a diode, or other rectifying component. The envelope detector self mixing efficiency falls off as the carrier power decrease. Thus the sensitivity for a TRF receiver is moderate compared to the super heterodyne with a mixer always being efficiently switched by a strong LO signal. However, the typical applications for Wake-up receivers require only rather short transmission range, up to about 10 meters [31]. Excluding the LO is well motivated by the achieved reduction in active power.

The envelope detector folds the modulated spectrum around the carrier f_0 down to baseband frequency f_m, see Fig. 2.9. The baseband output voltage V_m from the envelope detector is proportional to the square of the input amplitude of the RF carrier V_{RF},

$$V_m \propto V_{RF}^2. \tag{2.1}$$

Boosting V_{RF} with a pre-amplifier in front of the detector would improve the sensitivity. It is worth to note that it is the carrier amplitude that is important, rather than carrier power, and that voltage amplification can be achieved passively by a transformer. It is difficult to get efficient voltage transformation with on-chip inductors, the large inductance needed would occupy large die area

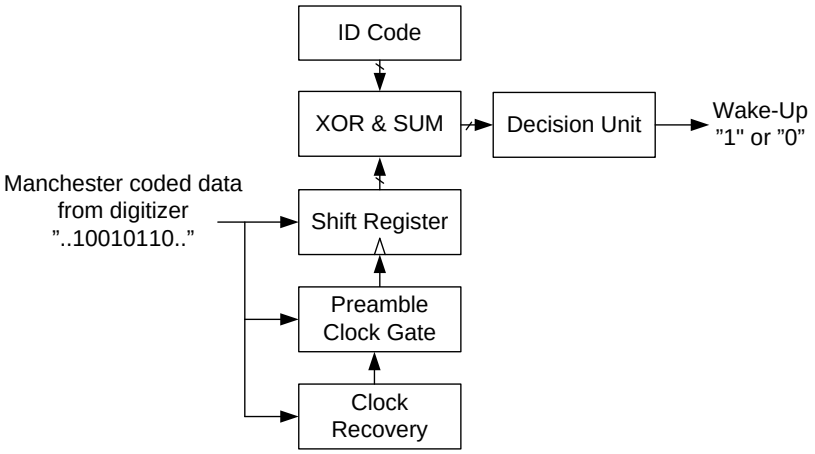

Figure 2.10: *Self-clocked correlator block diagram.*

and have a too low self resonance frequency. Lumped off-chip inductors would add to the component count cost and occupy valuable bonding pad resources for terminals. Further, the transmission lines and bond wires used to connect the inductor have to be taken into account during design, and they are proven to be difficult to control. A distributed passive transformer may be a way around the problem without adding any components to the design. High Q-values are available with modern laminate materials, even a low cost material as FR4 will suffice.

The output from detector is amplified to ensure safe switching in a digitizer. As the detector output at weak input carrier levels falls of very quickly the baseband processing must be designed for low noise performance. A low baseband bandwidth enables subthreshold biased transistors to be used in the design and ensure low power consumption.

Immunity to interfering radio signals is important for Wake-up radios. As the basic sensitivity is not affected by an inband blocker signal, we anticipate that a receiver using this envelope detector can operate also in the presence of an inband blocker considerably larger than the signal itself [32]. The only effects of a blocker is 1) its amplitude modulation will affect the receiver if that spectrum falls within the baseband spectrum used by the receiver, and 2) it may convert a large input RF-noise to noise in the receiver baseband. In addition, intermodulation products between the blocker and the signal may affect the receiver, depending of their respective spectra.

ID-code correlation

The baseband digital signal processing requires a baseband clock. Although this clock will run at a significant lower frequency than the LO it will consume energy, and require external resonating elements such as crystals, or capacitors, and a periodical re-synchronization such as a phase locked loop. The baseband clock can instead be embedded in the transmitted data. If no phase locked loop or other flywheel function is included the clock must be transferred together

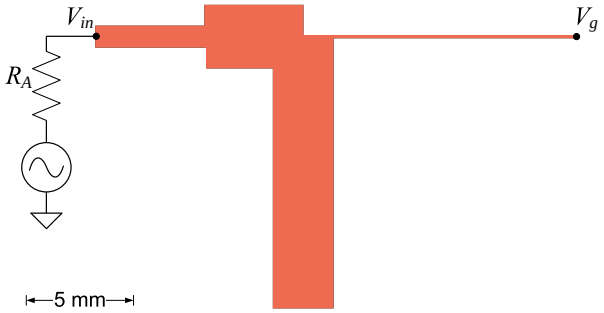

Figure 2.11: *Layout of the RF voltage transformer metal pattern on PCB.*

with each data bit. Manchester coding enables this by coding each ID-code bit with a transition; the bit value "1" is coded with a "01"-transition, and bit value "0" is coded with a "10"-transition [33]. The cost is a doubled edge rate but the gain is, again, a simplified design. The actual bandwidth of the baseband signal is not increased but shifted upwards, reducing the impact of 1/f-noise [34]. Further, the baseband signal will be DC-free and the baseband circuitry would not need to have any DC-gain. DC level fluctuations from the detector are blocked out from the baseband amplifier by a DC-block capacitor.

A self clocked correlator, see Fig. 2.10, compares the received data with the stored ID. Data would be shifted in to a shift register by the recovered clock encoded in the Manchester data. A short preamble bit pattern is used to trigger the clock recovery circuit to start up. This would reduce the activity of the digital logic and save spending of dynamic energy. The length of the ID-code typically is around 100 bits. The EPC transponder Class 3 use 96 bits [35]. After Manchester encoding and addition of preamble the result is around 200 bits to transfer over the air interface. One thousand units may be addressed within one second with a bit rate of 200 kbps.

RF voltage transformer

An RF voltage transformer was placed on the same FR4 PCB carrying the die. The matching network was designed for a 0.508 mm thick FR4 laminate, see Fig. 2.11, and consisted of a 50 Ω transmission line leading to a single stub combined with a transmission line. Further, a bias network (not depicted in Fig. 2.11) for biasing of the detector via the RF input pad was attached to the transformer.

If a planar antenna (e.g. integrated to the carrier substrate) is used, its impedance is likely to differ from 50 Ω. That is not a major concern, it merely calls for a different design of the matching network.

Baseband amplifier

Baseband amplification was performed by two cascoded amplifiers with feedback connected in series, see Fig. 2.12.

The detector signal is very weak and we do not want the baseband amplifier to dominate the noise budget. Therefore the baseband amplifiers have to be

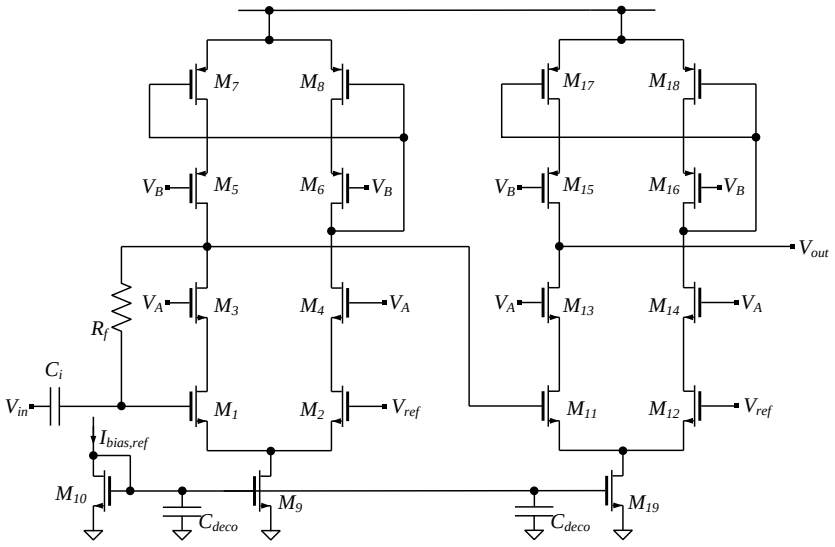

Figure 2.12: *Schematics for baseband amplifier with bandpass characteristics.*

designed for low noise performance. The largest noise contributor is the input transistor M1 of the first amplifier stage.

The filter topology chosen have a bandpass characteristic and requires a high resistive path, R_f, and a DC-blocking capacitor C_i. The high resistance in the feedback ensures a high input impedance towards the detector. The resistor R_f is set to 65 MΩ, and is implemented with the channel resistance of a subthreshold biased MOST.

A source follower amplifier (not depicted in Fig. 2.12) was added to the design as buffer for measurement purposes. The buffer amplifier adds no voltage gain but is capable to drive larger currents and isolates the baseband amplifier from the capacitive and resistive loading of the bonding pad and measurement equipment.

2.3.2 Results and discussion

The receiver was fabricated in a 130 nm CMOS process with MIM capacitors. No external components were used other than an etched transformer in the FR4 carrier PCB. The integrated circuitry, see Fig. 2.13, was fitted within an area of around 7000 μm^2 and is hence suited to be used as an IP-block being placed in a die corner, or near the die edge, of a general ASIC. The receiver was designed for 1 V bias to enable a low power design. For the same purpose all devices are operating in moderate or weak inversion. The total current consumption of the detector and baseband amplifier is 2.3 μA.

The receiver sensitivity was measured with a 2450 MHz carrier signal modulated with 100% ASK. The best sensitivity, P_{in}=-48.5 dBm, is found at f_{in}=2520 MHz, which corresponds to the best matching response from the transformer.

The proposed design is very resilient to interfering sources with a modulation spectrum outside the baseband amplifier bandwidth. Further, the use of a passive transformer for amplification makes the design robust against satura-

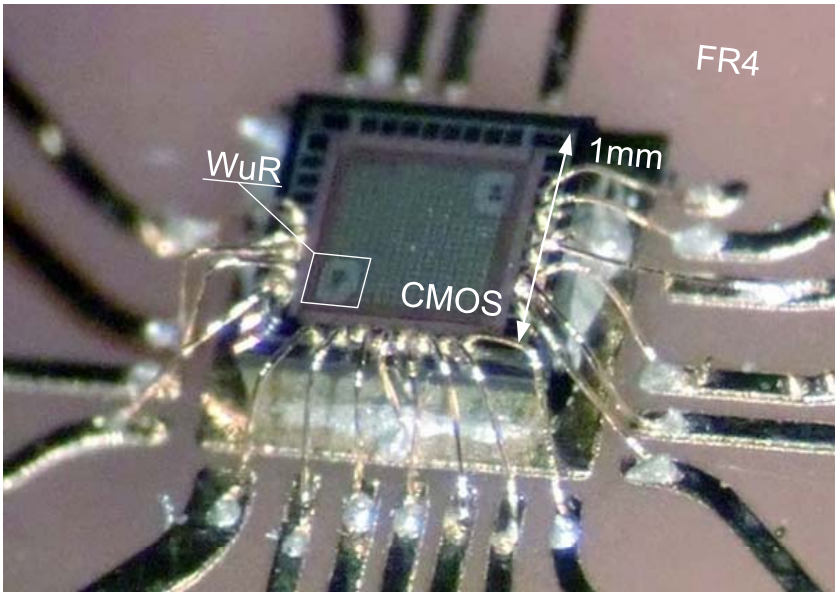

Figure 2.13: *Die photo of WuR implemented in a CMOS 130nm process and mounted on FR4 carrier substrate.*

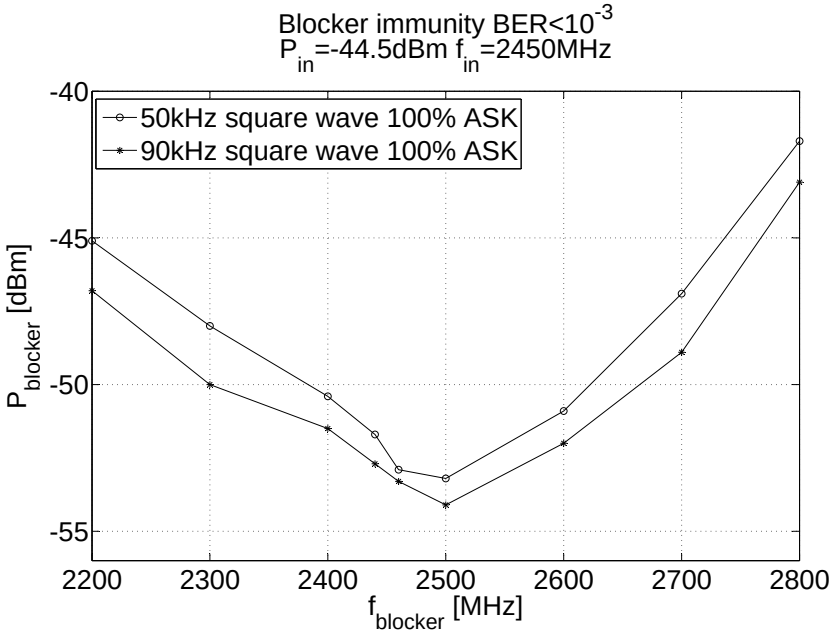

Figure 2.14: *Measured immunity to modulated blocker signal.*

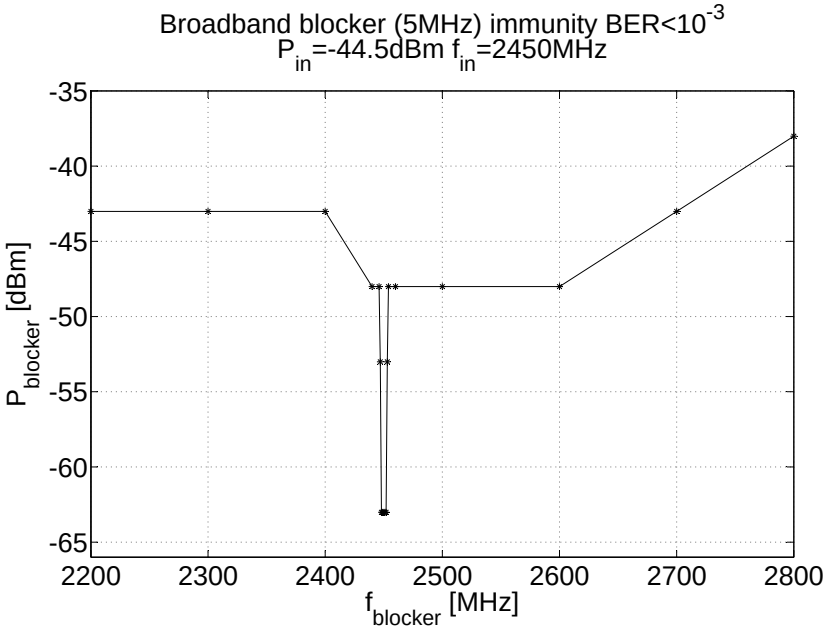

Figure 2.15: *Measured immunity to broadband 64QAM modulated blocker signal (simulating WLAN).*

tion and signal intermodulation caused by any overdrive of active components. A CW blocker signal with a level of -13 dBm only 1 MHz below the carrier did not swamp the sensitivity of the radio. During these measurements the modulated carrier signal, at 2450 MHz, was fixed at a power 3 dB above the required level for a BER=10^{-3} without interference. Interestingly the sensitivity can be improved by a CW interferer, and a sensitivity of P_{in}=-57.5 dBm was measured with a -20 dBm CW blocker 1 MHz below the carrier frequency. This improvement falls off rapidly as the blocker frequency moves out from the carrier frequency, and the receiver is virtually unaffected.

The result from the same set up, but with a modulated blocker, is presented in Fig. 2.14. As long as the modulated interferer power was roughly 6 dB below the sensitivity limit level the Wake-up radio was not blocked.

A particularly important blocker is a WLAN signal, also utilizing the ISM-band. Therefore the effect of a WLAN signal was tested, simulated as a 64QAM modulated signal with 5-MHz bandwidth, see Fig. 2.15. We note that for a WLAN signal we can accept up to -48 dBm blocker power without loss of sensitivity (except when the blocker is located within 2.5 MHz from the wanted carrier). The reason is that the baseband amplifier catches only a limited part of the 5-MHz WLAN spectrum, so not only the RF selectivity but also the baseband selectivity helps to suppress blockers.

A successful Wake-up radio solution has to be low cost and preferably work as an IP block to be included in several applications. This implies a single chip design in a commercially available CMOS process, and a use of low cost materials [15]. Further, the design needs to be robust in terms of process parameters variations, as well as environment variations and radio interference [36][32][37].

The presented design offers a robust and trim-free solution easily implemented in a CMOS process.

The implementation of low-power TRF receivers requires many and complicated trade-offs, and the question remains if it is possible to push the receiver energy efficiency even further? A structured analysis of the lower bound for Wake-up receivers energy consumption would be a valuable support for designers of modern radio systems.

2.4 Analysis of lower bound for WuR energy consumption

In the survey presented in Fig. 2.4 a lower bound for the attainable energy consumption per received bit is discernible, but what is the fundamental reason for this bound? Among the requirements driving power consumption are baseband bandwidth, sensitivity, and also carrier frequency and interference [32]. By studying basic receiver circuits it is possible to provide an overview of the first two of these mentioned requirements (baseband bandwidth and sensitivity) and to provide an intuitive picture of their relations to power consumption. The TRF receiver, with and without a preceding LNA, and the superheterodyne receiver are treated in the following analysis. The regenerative and super-regenerative receiver will not be analyzed analytically here, but are included in the survey presented in Fig. 2.4.

2.4.1 Description of parameter set and analysis

Noise in a linear system may be calculated with Friis cascade formula for noise figure F,

$$F = F_1 + \sum_j \frac{F_j - 1}{\prod_{i<j} G_i^2}, \tag{2.2}$$

where F_j and G_i is the noise figure and voltage gain respectively for each stage in the cascaded system. The assumption of linearity is valid for most receiver building blocks at low power signal levels, with the detector as an exception. Analysis for the envelope detector (ideal squarer) can be found in [32], [38].

For the analysis it is necessary to choose reasonable parameter values. These values may be updated as technology development continues. The component values, or the parameter set, used in the following is meant to reflect typical values for integrated CMOS fabrication processes, and typical small sized RF lumped components. Normally the number of discrete components is a strong driver of cost, so we look for single chip solutions with a minimum number of external components. The minimum output SNR for reliable detection is assumed to be 12 dB [15].

90nm CMOS is chosen as reference technology, using the same basic parameters as in [39] ($C_{min} = 1$ fF and effective voltage $V_0 = 75$ mV). On-chip inductors rarely reach higher inductance values than 10 nH or a better Q than 5 [22]. Further, the loading capacitance of an ASIC bond pad end up at around 400 fF when ESD protection is included. Here it is assumed that we may reduce the load to 75 fF, reflecting the ongoing development of RF ESD clamps [40].

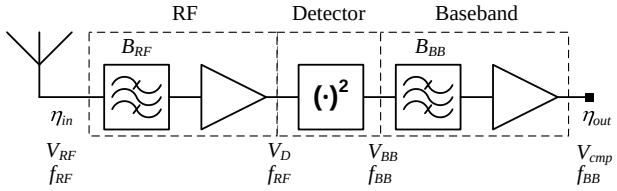

Figure 2.16: *Tuned RF receiver (TRF). Signal-to-noise ratio is symbolized with* η

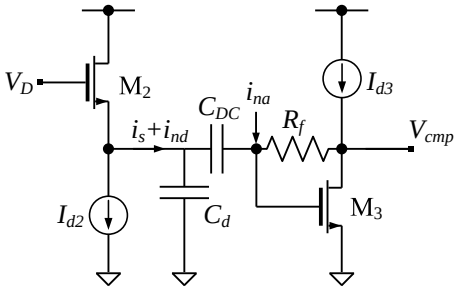

Figure 2.17: *RF-detector and transimpedance amplifier (TIA).*

External inductors display a Q of around 35 for inductance values available with a serial resonance above the carrier frequency we look into. Further the baseband noise bandwidth B_{BB} is assumed to be twice the bit rate of the receiver (i.e. the bit rate 250 kbps require a baseband bandwidth of $B_{BB} = 500$ kHz). Furthermore the temperature is assumed to be $T = 300$ K. Finally, a supply voltage of 1 V is used in the analyzed designs. Supply voltage may be as low as 0.5 V, but it will not change the conclusions.

Tuned RF receiver

A block schematic of a TRF receiver is found in Fig. 2.16. In the TRF the received signal is bandpass filtered around the intended RF center frequency, f_{RF}, with a bandwidth B_{RF} to reduce impact from out of band interfering signals. The RF-filter of a Wake-up radio usually is broadband, to make it robust against process variations and to add a minimum of loss. The antenna itself is likely to be resonant and may provide sufficient selectivity. The inclusion of an RF pre-amplifier is optional, and depend on the targeted receiver sensitivity. Amplification of the signal before detection increases the sensitivity, but has a substantial impact on the power budget since RF gain is expensive from a power perspective.

The most basic implementation of the TRF is an envelope detector followed by a baseband amplifier, see Fig. 2.17. Basically this is an integrated version of the vintage crystal radio, where the incoming radio signal voltage V_D drives a detector transistor M2 instead of a crystal diode. The outgoing detector current i_s is filtered by a detector capacitor C_d before being amplified in a transimpedance amplifier consisting of transistor M3 and feedback resistor R_f. Capacitor C_d also acts as a low impedance path to ground for the radio signal.

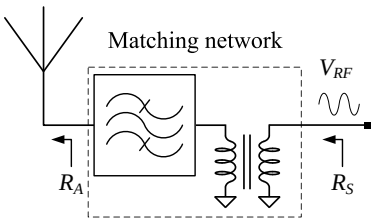

Figure 2.18: *RF-transformer with input impedance R_A and output impedance R_S and passive voltage gain $G_T = \sqrt{R_S/R_A}$. The transformer also works as a matching network and a filter*

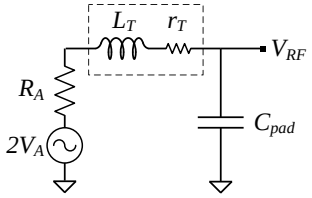

Figure 2.19: *RF-transformer with external inductor in series with the capacitance of the chip RF input port*

Noise from the detector is represented by the current i_{nd}, while amplifier noise is represented by the current i_{na}. The outgoing voltage V_{cmp} is digitized in a comparator, or by an ADC. Bias currents for the transistors are I_{d2} and I_{d3}.

With an up-transforming network between the antenna and the detector the sensitivity is improved. A passive up-transformer works by trading current for voltage amplitude and thus increases the (usually) low antenna impedance, R_A, to a higher value, R_S, see Fig. 2.18. With a sufficiently small detector transistor the MOS gate input impedance will be high and the achievable transformation ratio will rather be limited by the Q-value of the resonating elements. This is illustrated with the straightforward impedance transformer circuit consisting of an external inductor in series with the chip RF input port, see Fig. 2.19. The external inductor with inductance L_T has a finite Q represented by a series resistance r_T. Matching is achieved at resonance if we choose r_T to be equal to antenna resistance R_A. The voltage at the chip input is $V_{RF} = QV_A$, and the passive voltage gain becomes $G_T = Q$. With an RF port pad capacitance $C_{pad} = 75$ fF and a target resonance frequency of 2.5 GHz the inductance L_T becomes 54 nH. Now, with an antenna impedance of 50 Ω the inductor Q equates to roughly half the assumed achievable value of 35 in our parameter set. However, this is readily solved by reducing the antenna impedance by a factor of two since small sized antennas in any case are known to have a low radiation resistance [41], thus leading to antenna impedance $R_A = 25$ Ω and a Q of 35.

We obtain the following expression for outgoing SNR of the TRF without LNA,

$$\eta_{out} = \frac{\left(I_{d2}V_D^2/(4V_0^2)\right)^2}{4\gamma kTB_{BB}I_{d2}/V_0 + \dfrac{16\pi^2 kT\gamma C_d^2 B_{BB}^3}{3I_{d3}/V_0}}, \tag{2.3}$$

where V_0 is the efficient voltage of the transistors and k is Boltzmanns constant. The transistor noise parameter γ is henceforth approximated with $\gamma = 1$, for better readability of expressions.

The optimum distribution of the two bias currents I_{d2} and I_{d3} in this receiver depends on targeted sensitivity, and the relation may actually be better perceived if we instead look at the inverse of (2.3),

$$1/\eta_{out} = \frac{64kTB_{BB}V_0^4}{V_D^4}\left(\frac{1}{I_{d2}V_0} + \frac{4\pi^2 C_d^2 B_{BB}^2 V_0}{3I_{d3}I_{d2}^2}\right). \tag{2.4}$$

Here two terms are being functions of the bias currents, each term dominate the SNR calculation within different intervals of sensitivity. The goal for a designer is to find a distribution of bias currents with minimum total current, $I_{tot} = I_{d2} + I_{d3}$, while still passing the SNR threshold resulting in a BER=10^{-3}. If we look at the two terms in (2.4) isolated one at a time, the expected behavior of an overall optimization may be foreseen. The first term of (2.4), dominates the power budget for higher sensitivities, and is plotted as energy-per-bit in Fig. 2.20 with the total bias current going through the detector ($I_{d2} = I_{tot}$). In this domain detector noise is prevailing, and DC-power should be spent on detector biasing. The RF sensitivity in Fig. 2.20 is calculated with $G_T = 35$ and $R_A = 25\ \Omega$. The second term of (2.4) dominates the power budget at low sensitivities, and it can be showed that this term is minimized when $I_{d3} = I_{tot}/3$. In Fig. 2.20 the second term is plotted as energy-per-bit with this optimized current distribution. In this domain the baseband amplifier noise prevails and thus the DC-power should be diverted from the detector to the baseband chain instead.

This is also an expected result from (2.2) where the noise figure of the first stage, if having enough gain, will dominate the overall system noise figure.

The overall power optimization of the receiver is graphically presented in Fig. 2.20. The optimized curve makes a smooth transition between the two sensitivity intervals.

The energy-per-bit for the TRF receiver without LNA is independent of baseband bandwidth. When the first term in (2.4) dominates SNR, η_{out} is proportional to I_{tot}/B_{BB} (energy-per-bit). With the second term dominating η_{out} is proportional to $(I_{tot}/B_{BB})^3$ (the cube of energy-per-bit).

Boosting V_{RF} with a pre-amplifier, beyond what is possible with a passive impedance transformer, would improve the receiver sensitivity drastically. However, it is not obvious at what level of sensitivity the pre-amplifier pays off in our power budget.

In Fig. 2.21 a TRF with LNA is depicted. The baseband amplifier is here skipped for simplicity. LNA noise is represented by the voltage $V_{D,n}$, while outgoing noise from the detector is represented by i_n.

The LNA has a resonant load providing narrow band amplification at a carrier angular frequency $\omega_{RF} = 2\pi f_{RF}$, and thus also offer some RF filtering. The expression for the RF gain with a resonant load having quality factor Q_L is,

$$G_{RF} = g_{m1}R_L = \frac{g_{m1}Q_L}{\omega_{RF}C_{L1}}, \tag{2.5}$$

where g_{m1} is the transconductance, R_L is the load impedance, and C_{L1} is the capacitive load from subsequent stages and possible tuning capacitors.

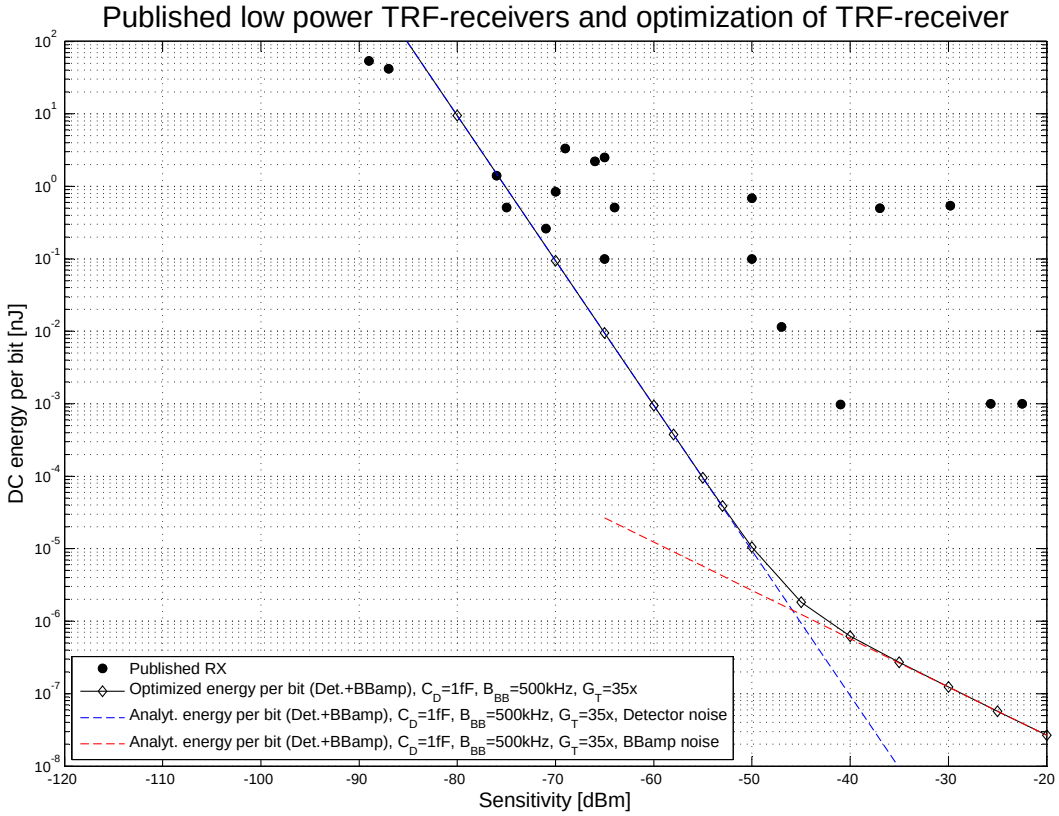

Figure 2.20: *The baseband amplifier and detector dominate power budget at different sensitivity intervals. Curves are calculated with (2.4) and are independent of baseband bandwidth B_{BB}. The available RF power (sensitivity) is calculated using the series transformer in Fig. 2.19 with $Q = 35$, and an antenna impedance $R_A = 25\ \Omega$. TRF receiver data from Fig. 2.4 is plotted for comparison.*

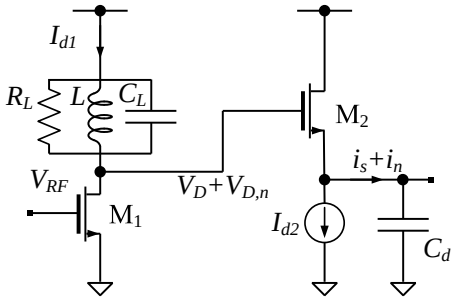

Figure 2.21: *RF-detector and LNA with amplification G_{RF}.*

The expression for output SNR (again inverted) of the complete TRF receiver with the LNA included and as a function of biasing currents is,

$$1/\eta_{out} = \frac{32kTB_{BB}}{V_{RF}^2}\left(2\frac{V_0^7(\omega_{RF}C_{L1})^4}{I_{d2}I_{d1}^4V_{RF}^2Q_L^4} + \frac{V_0}{I_{d1}}\right). \tag{2.6}$$

We identify two different terms dominating the power budget at different sensitivity intervals. With typical on-chip low Q inductors and for reasonable sensitivities the first term, representing detector noise, will dominate over the second term, representing converted noise from the LNA transistor M1. It can be shown that the bias current distribution that minimizes the first term is $I_{d1} = 4/5I_{tot}$, where $I_{tot} = I_{d1} + I_{d2}$. The result depends on the baseband bandwidth in this case. The improvement with an LNA is significant for higher sensitivities, while at lower sensitivities the LNA becomes superfluous. The sensitivity level where the pre-amplifier pays off depend on targeted bandwidth (i.e. bit rate).

With a resonant load the amplifier performance is limited by the inductance and the Q-value that is possible to achieve with on-chip inductors. The achievable inductance also imposes a lower limit on the capacitive load if resonance should be attained. If we instead look at a pure resistive load the capacitance can be minimized $C_{L1} = C_{min}$. We can now easily modify (2.6) with Q set to unity,

$$G_{RF} = g_{m1}R_L = \frac{g_{m1}}{\omega_{RF}C_{L1}}, \tag{2.7}$$

where we have used the bandwidth requirement $R_L = 1/(\omega_{RF}C_{L1})$ limiting the load resistor size [39]. We get,

$$1/\eta_{out} = \frac{32kTB_{BB}}{V_{RF}^2}\left(2\frac{V_0^7(\omega_{RF}C_{min})^4}{I_{d2}I_{d1}^4V_{RF}^2} + \frac{V_0}{I_{d1}}\right). \tag{2.8}$$

If we have the opportunity to place the inductance of the resonant LNA outside the chip, some advantages can be noted. First, we may increase the inductance value, giving a higher load impedance. Second, the Q of an external inductor is normally better due to larger size and a better isolation from lossy substrate material. However, we also note some complications with this procedure. The typical bond pad parasitic capacitance limits the size of applicable inductors (since resonance frequency of the amplifier load is $\omega_0 = 1/\sqrt{LC}$). Further, the process of bonding and contacting external components complicates the implementation and make it technically challenging.

We conclude that the overall power consumption is reduced with the higher Q offered by an external inductor, and that the LNA continues to contribute to reduction of power down to lower sensitivities. However, we also note that an external inductance can not compete with the performance of a cheaper and technically less complicated on-chip resistive load, see Fig. 2.24.

It is here relevant to mention active inductors as an alternative to passive inductors. The voltage gain of an LNA with an active inductor, see Fig. 2.22, with transconductance g_m and a capacitive load C_L, can be shown to be $A_V = (g_m/(\omega C_L))^2$. If we look for a voltage gain of say A_V =10, this corresponds to a transconductance of 50 μS with the minimum capacitance C_{min} at the frequency 2.5 GHz. A resistive load requires a $\sqrt{A_V} = \sqrt{10}$ times larger conductance under the same conditions, equating to 157 μS. Taking into account the added noise

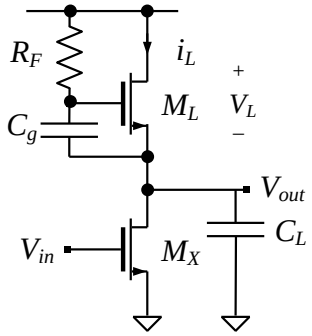

Figure 2.22: *Amplifier with active inductive load.*

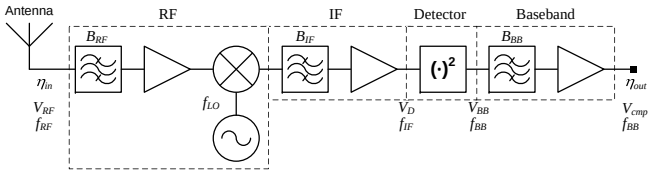

Figure 2.23: *Superheterodyne receiver (SHET).*

associated with active inductors the net improvement is rather small. The use of an external inductance with Q =35 resonating together with a pad-capacitance of 75 fF would require a transconductance of 337 μS to achieve the same gain.

Superheterodyne receiver

One of the most widely used radio receiver architectures is the superheterodyne, depicted in Fig. 2.23. It differs from the TRF by a down-converting stage that reduces signal frequency before the actual detection take place. Among the primacies of the superheterodyne we find a high sensitivity and well controlled channel filtering. Further, the amplification at the IF require less DC-power. On the other hand, the down-converting mixer stage needs to be driven by a LO that constantly drains the power supply. The superheterodyne receiver may be tuned to different RF channels by shifting the LO frequency. A negative consequence of this tuning ability is that the superheterodyne is sensitive to LO frequency instabilities, but this problem can be mitigated by using a more tolerant IF-stage design [15].

We have studied oscillator realizations using an RC-tank circuit and LC-tank circuits. RC-oscillators have the advantage over LC-oscillators of being easier to integrate on chip since they have no large inductor consuming expensive silicon area. One major drawback is that the lossy RC-network implies a higher power consumption and lower Q leading to increased phase noise as compared to an LC-oscillator. Although ASK modulation is not phase sensitive, the phase noise of the LO may reduce SNR by converting adjacent channel interferers into the baseband [42]. An overview of the oscillator bias currents is found in Table 2.2.

Table 2.2: Estimated critical currents for oscillator implementations

Implementation	Resonant tank parameters	I_{crit} [μA]
LC on-chip	$C = 400$ fF, $L = 10$ nH, $Q = 5$	637
RC on-chip	$C = 1$ fF, $R = 63.7$ kΩ	23.6
LC off-chip	$C = 75$ fF, $L = 54$ nH, $Q = 35$	16.8

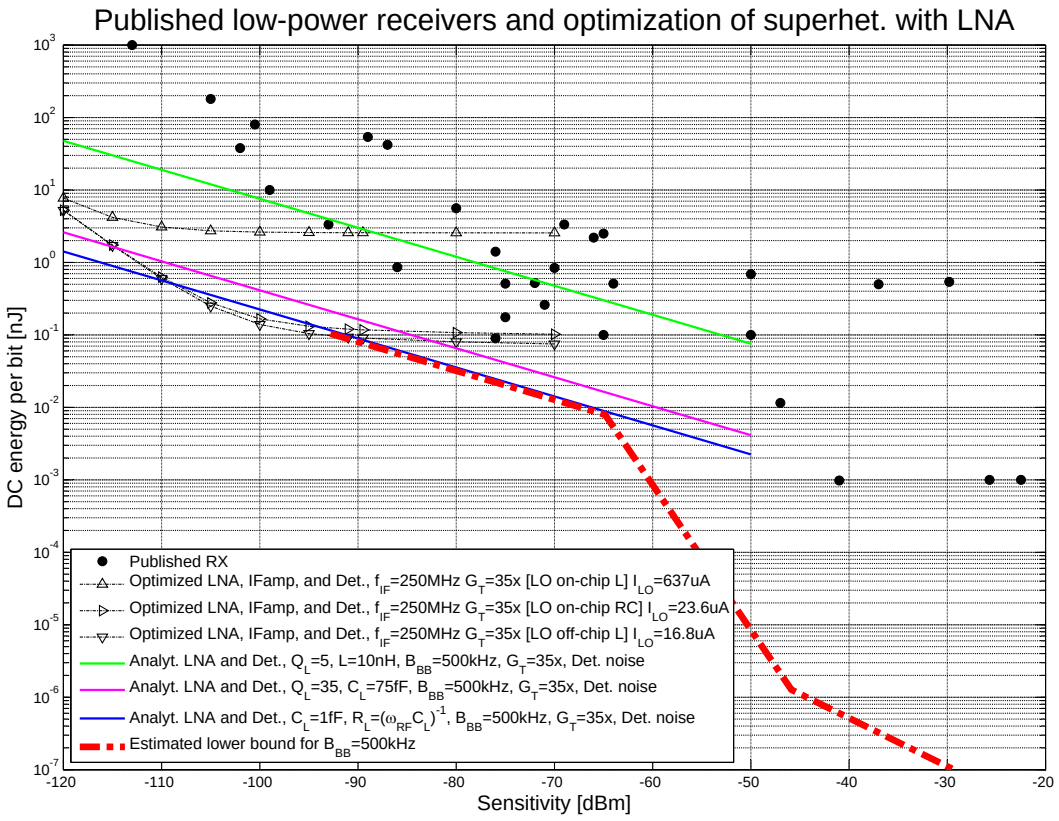

Figure 2.24: *The red dotted line is the best estimate of the lower bound to power consumption at baseband bandwidth B_{BB}=500 kHz for any receiver architecture (the line stops at the antenna noise limit). Data for all receivers from Fig. 2.4 is plotted for comparison. Energy-per-bit for the superheterodyne with LNA (triangles). The impact of the mixer noise is reduced by the use of an LNA. The LO supply power add a lower floor on energy-per-bit performance at low sensitivities. With wider baseband bandwidths, B_{BB}, this floor will be pushed downwards. Other lines show energy-per-bit for TRF with preceding LNA using different loads.*

2.4.2 Results and discussion

The above analysis does not take into consideration the use of cascade amplifier stages. An amplifier block may consist of multiple $K+1$ stages in a chain, where gain factors are multiplied and bias currents are summed. Only the first stage in the cascade has to be optimized for noise, with say a current I_{dn}. Subsequent stages may instead be optimized for maximum gain. If we assume equal amplification in each subsequent stage of the cascade, and each stage has a gain proportional to their individual bias current I_{dk}, then the total amplification of the subsequent cascade is proportional to I_{dk}^K and the total bias current is $I_d = KI_{dk}$. If we modify our expressions for gain according to this we have,

$$G = \frac{I_{dn}}{V_0} R_L \frac{I_{dk}^K}{V_0^K} R_L^K = \frac{I_{dn} I_{dk}^K R_L^{(K+1)}}{V_0^{K+1}} \tag{2.9}$$

This extension of our analysis would result in somewhat lower bounds but will not change our general conclusions. The threshold for a total gain G where it is appropriate to switch from a design with $N-1$ stages to a design with N stages in a cascade is,

$$G = \left(\frac{N}{N-1} \right)^{N^2-N}. \tag{2.10}$$

Thus a two stage amplifier should be considered when the total voltage gain exceeds 4x. The TRF receiver has its amplification concentrated to the LNA, and the here treated receivers use a maximum gain of $G = 20$x before the antenna noise limits the sensitivity. With this level of gain it is justified with three amplifier stages in the LNA. With a growing number of stages and with higher sensitivity the inherent noise of the amplifiers will become evident. This noise will be amplified by all the subsequent stages.

The result of the analysis is that a simple envelope detector is preferred for low sensitivities, above signal levels of about -70 dBm. For higher sensitivities the envelope detector should be preceded by an LNA for better energy efficiency. In no case the more complicated super-heterodyne offers a clear benefit. The lower bound of energy per bit is controlled both by transistor performance and passive device performance, and for the conditions examined inductor passives are beneficial for antenna impedance transformation only. The predicted lower bounds are one order of magnitude lower than the best published data for high sensitivities considering carrier frequencies above 500 MHz, and several orders of magnitude lower for low sensitivities over all carrier frequencies. The presented method for power bound predictions can be extended to include all kinds of RF systems and also include other performance measures as selectivity, linearity, etc.

Chapter 3

A microwave based imaging sensor

While in communication the interaction between wave and matter in the channel is largely unwanted, this is exploited in electromagnetic sensor applications. Microwaves are used for remote sensing in radiometry, temperature measurements, gas analysis, and in radar and astronomy. When the sensed object is relatively close to the sensor (i.e. within the last 10 meters) the transmitted power can be very low, down to a few micro-Watts. Many metrics can thus be acquired without having the sensor in situ. This is attractive in many industrial applications, where the environment often is harsh and maintenance cost otherwise would be prohibitively high. This chapter describes an experimental setup of a radar interferometer inside a blast furnace producing hot metal for steel production.

3.1 Background

3.1.1 Contact free measurements with radar

Radar was developed during 1930s and 1940s and is known for its important role during World War II as an early warning system before aerial attacks [27] [28]. By measuring the round trip delay of an electromagnetic pulse it is possible to determine the distance to a remote object. By using repetitive pulses, the speed of the object can be measured as the relative difference in range between two pulses. The pulse repetition frequency determines the farthest range that can be measured without any ambiguity in distance, while the pulse duration gives the resolution of the pulse radar. Radar has the ability, in contrast to laser, to see through dust, fumes, and walls. The long waves even makes it possible to see around corners, such as in a curved tube or shaft. Pulsed radar is usually used for low cost applications, and is an incoherent technology, meaning that it is only able to detect the power of the pulse.

Another cost effective radar technology is Frequency Modulated Continuous Wave (FMCW) radar. The resolution of the FMCW radar system depends on its effective pulse length T_{eff}, where a shorter pulse length gives a higher resolution. If the signal-to-noise ratio (SNR) is to be unchanged the peak power of the pulse

has to increase as the pulse length gets shorter. However, the available peak power is limited by radio frequency (RF) electronics, such as power amplifiers, which may be driven into their nonlinearity region or signal levels where they are damaged. If the energy of the pulse is spread over a longer period of time, T_{pulse}, the peak power is reduced but the SNR is preserved. In the FMCW radar this distribuion over the time domain is achieved by chirping the radar pulse. The pulse can, after reception, be compressed by a matching filter to an effective duration time T_{eff}. The chirp can be realized with an analog frequency sweep or by a stepped frequency sweep. In the stepped frequency sweep the pulse can be shaped synthetically by a discrete Fourier transformation of the signal. For a uniform chirp over bandwidth f_{BW}, the 3-dB level pulse length T_{eff} is [43],

$$T_{\text{eff}} \simeq \frac{0.886}{f_{\text{BW}}}, \tag{3.1}$$

and we get the radial resolution,

$$\Delta R_{\text{eff}} = 0.443 \frac{c_0}{f_{\text{BW}}}. \tag{3.2}$$

The stepping size of the frequency is $f_{\text{step}} = f_{\text{BW}}/N_\omega$, where N_ω is the number of frequency points. This sampling rate in the frequency domain gives a maximum target range that can be determined without ambiguity. The frequency samples do not necessarily have to be evenly distributed or even in a falling or rising sequence. Incomplete frequency coverage will however cause sidelobes of the pulse. Among FMCW radar applications are tank- and levelling radars, altimeters and automotive radars. The FMCW radar is a coherent radar technology, meaning that it uses the phase information of the radar pulse.

The angular resolution of an antenna is limited by its aperture size. If the radar system is placed on a moveable sensor platform, such as an aeroplane or a satellite, a larger antenna aperture can be synthesized, by combing signals from several positions during the movement of the platform.

The reflection from targets are positioned in range by the transmission and reception of a chirp, or pulse. Different radial directions give different doppler shift as the platform moves. The radial spheres and doppler cones form a coordinate grid on the ground. This coordinate grid, gives a 2D imaging technique.

Several combined SAR systems with a slightly shifted flight path, or a combination of several passes can form an interferometric 3D image. Then the baseline is formed by the distance, measured perpendicular to the moving direction, between the systems or passes. This technique has been used to make elevation maps of the earth surface [44], and elevation changes caused by different geological activities [45]. Applications are geodesy, ice mapping, military, and environmental surveillance.

3.1.2 Interferometry

Radio interferometry has been successfully used in astronomy research for decades and is known to produce high resolution images of the sky brightness distribution. Radio waves can reveal objects that are not visible in the optic range due to clouds of cosmic dust. This measurement technique may also be adopted for use in industrial environment on the ground.

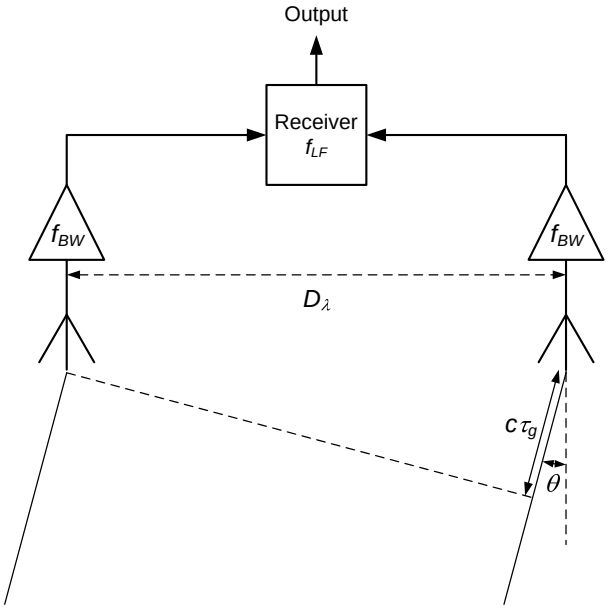

Figure 3.1: *Elementary interferometer showing bandpass receiver amplifiers, the geometric time delay τ_g (c is speed of light), and the receiver with lowpass filter bandwidth f_{LF}. Distance between antennas, D_λ, is measured in wavelengths.*

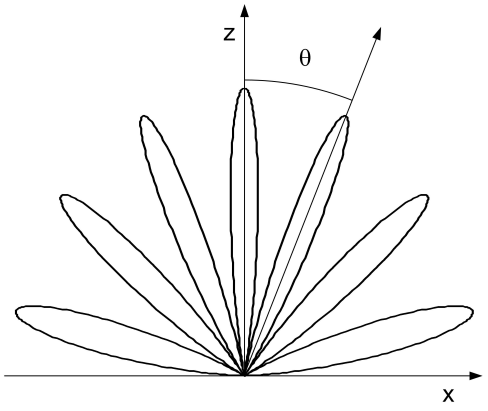

Figure 3.2: *Intensity sensitivity pattern for a two element interferometer.*

The two element interferometer compares the signal information from two receiving antennas, see Fig. 3.1. By measuring the phase shift between the signals, the difference in travelled path length for the received waves is estimated. If the distance between the antennas, $D = D_\lambda \lambda_0$, is known we can calculate the angular position θ of the signal source. The distance D is called the interferometer baseline. $D_\lambda = |\boldsymbol{D}_\lambda|$ is the baseline expressed in number of wavelengths. The geometrical time delay τ_g is,

$$\tau_g = \frac{Dsin(\theta)}{c_0} \tag{3.3}$$

The phase difference between the two received signals is,

$$\Delta\varphi = \tau_g c_0 \frac{2\pi}{\lambda_0} = 2\pi \frac{Dsin(\theta)}{\lambda_0} \tag{3.4}$$

where λ_0 is the free space wavelength of the radiation from the source. From 3.4 it is readily seen that the response from the interferometer, which is varying as $cos(\Delta\varphi)$, is repetitive if θ is allowed to sweep over a certain range. The periodic response is referred to as fringes, see Fig. 3.2. Because of this angular ambiguity, there is an uncertainty in which fringe lobe the source is situated.

The fringe visibility in the case of a Michelson interferometer is originally defined as,

$$V_M = \frac{intensity\ of\ maxima - intensity\ of\ minima}{intensity\ of\ maxima + intensity\ of\ minima}, \tag{3.5}$$

which is a real quantity normalized to unity when the intensity at minima is zero. This corresponds to an unresolved source, the source is small compared to the fringe lobe width. If we want to map asymmetric sources, a complex visibility function must be defined to represent the phase of the visibility. The source may be described by an intensity pattern $I(\boldsymbol{\sigma})$ where $\boldsymbol{\sigma}$ is the position vector relative to a phase-tracking center $\boldsymbol{s}_0$. The phase-tracking center, or phase reference position, is often placed in the middle of the source that is being mapped. With two antennas separated by a distance of $D_\lambda = |\boldsymbol{D}_\lambda|$ wavelengths, and with an interferometer bandwidth of f_{LF}, the correlator output is, according to [46],

$$r(\boldsymbol{D}_\lambda, \boldsymbol{s}_0) = f_{LF} \int_{4\pi} F(\boldsymbol{\sigma}) I(\boldsymbol{\sigma}) \cos\left[2\pi \boldsymbol{D}_\lambda \cdot (\boldsymbol{s}_0 + \boldsymbol{\sigma})\right] d\Omega \tag{3.6}$$

The complex visibility is then defined as,

$$\mathcal{V} = |\mathcal{V}| \exp^{j\phi_\mathcal{V}} = \int_{4\pi} F(\boldsymbol{\sigma}) I(\boldsymbol{\sigma}) \exp\left(-j2\pi \boldsymbol{D}_\lambda \cdot \boldsymbol{\sigma}\right) d\Omega, \tag{3.7}$$

where $F(\boldsymbol{\sigma})$ is the antenna normalized antenna pattern and $d\Omega$ is a infinitesimal source solid angle. The visibility $\mathcal{V}$ is a function of the projected baseline D_λ. When the baseline is expressed in number of wavelengths, $\mathcal{V}$ are samples of the source at the same spatial frequency

Synthesis mapping

With the assumption that the source is spatially incoherent, it is possible to derive the source pattern $I(\boldsymbol{\sigma})$ by a Fourier transformation of the visibility function

$\mathcal{V}$. The phase reference point $\boldsymbol{s_0}$ will be the origin of the synthesized intensity map. We further assume the interferometer baselines to be inside a plane, and that the distance to the source is very large (planar wave fronts). With a two dimensional coordinate system (l, m) of direction cosines with respect to the baseline coordinates (u, v) we can restate (3.7) as,

$$\mathcal{V}(u,v) = \int_{-\infty}^{\infty}\int_{-\infty}^{\infty} F(l,m)I(l,m)\exp\left(-j2\pi[ul+vm]\right)\frac{dldm}{\sqrt{1-l^2-m^2}}. \quad (3.8)$$

For a restricted range of l and m the inverse transform is,

$$\frac{F(l,m)I(l,m)}{\sqrt{1-l^2-m^2}} = \int_{-\infty}^{\infty}\int_{-\infty}^{\infty} \mathcal{V}(u,v)\exp\left(j2\pi[ul+vm]\right)dudv. \quad (3.9)$$

Deconvolution and the dirty beam

We use a synthetic beam for the mapping of the sky, or in our case for the mapping of blast furnace surface. The synthesis mapping convolves the beam around the sources off the target and we get a so called dirty map. The baselines of the interferometer samples the receiving aperture, and there might be large uncovered zones in the uv-plane. These uncovered zones, or holes, in the coverage, convert to sidelobes of the beam. If we know the interferometer spatial sensitivity function $W(u, v)$ [46] it is possible to deconvolve it from the dirty map. The measured visibility $\mathcal{V}'(u, v)$ is a two dimensional convolution,

$$\mathcal{V}'(u,v) = [\mathcal{V}(u,v) * *\bar{F}(u,v)]W(u,v), \quad (3.10)$$

where the bar denotes the Fourier transform. The measured intensity distribution is the Fourier transform of (3.10)

$$I'(l,m) = [I(l,m)F(l,m)] * *\bar{W}(l,m), \quad (3.11)$$

which is the convolution of the source with the interferometer beam $\bar{W}(l, m)$. Unfortunately a deconvolution is a rather ill-posed problem since we both have noise and zero passings in the beam $\bar{W}(l, m)$. There have evolved a number of nonlinear methods to solve this problem. A well known approach is the Wiener filter [47], that uses the statistics of the signal and the noise. Other methods are Maximum Entropy Method (MEM) [48] and CLEAN [49]. CLEAN is widely used in radio astronomy, but MEM has attracted a lot of research efforts and can be explained in a stricter mathematic sense. All these methods use the sampled information and try to estimate the most likely or reasonable data values where information is missing. In the coherent case it is necessary to consider the phase pattern of the beam when making the deconvolution, since interference can cause false peaks or nodes in the intensity map, known as speckle. There exist modified versions of CLEAN that handle this by choosing among several estimates and, by a tree algorithm, following the most probable route down to a final image [50].

Measurement data $\mathcal{V}'(u, v)$ is the true data $\mathcal{V}(u, v)$ being sampled with a non-regular beam $W(u, v)$. The true image $I(l, m)$ is the Fourier transform of $\mathcal{V}(u, v)$. However in the real world a noise component $N(u, v)$ always is present and (3.10) should be altered accordingly,

$$\mathcal{V}'(u,v) = [\mathcal{V}(u,v) * *\bar{F}(u,v)]W(u,v) + N(u,v). \quad (3.12)$$

With a Fourier transform we get

$$I'(l,m) = [I(l,m)F(l,m)] * *\bar{W}(l,m) + \bar{N}(l,m), \tag{3.13}$$

The deconvolution problem is to find $I(l,m)$ in the presence of the noise. A direct method, *Fourier-quotient method*[47], is described by,

$$\tilde{\mathcal{V}}(u,v) = \frac{\mathcal{V}'(u,v)}{W(u,v)} = \mathcal{V}(u,v) + \frac{N(u,v)}{W(u,v)}, \tag{3.14}$$

here and in the following $F(l,m)$ is supposed to be constant and unity for a simplified discussion. This method can not be used in the presence of noise if zeros occur in $W(u,v)$, which is the case in interferometry. When the zeros occur the noise becomes infinitely amplified. Below follows a description of other methods that has been developed to circumvent this problem.

A linear and regularized methods is to minimize an error function [47],

$$J(I) = ||I'(l,m) - \bar{W}(l,m) * *I(l,m)|| + \lambda||\bar{H}(l,m) * *I(l,m)||, \tag{3.15}$$

where $H(u,v)$ is a highpass filter. The solution to this is,

$$\tilde{\mathcal{V}}(u,v) = \frac{W^*(u,v)\mathcal{V}'(u,v)}{|W(u,v)|^2 + \lambda|H(u,v)|^2}. \tag{3.16}$$

By numerical methods the optimal λ value is found. The resulting images are smoothed. Generalization of this method gives the *Wiener Filter*. It is necessary to includes statistics of the present noise and the signal to be measured.

The CLEAN method was developed to solve the problem of high sidelobe levels from non-regular baseline distributions in radio astronomy interferometry, [49],[47] and [46]. It assumes the image to be composed by point sources. It iteratively finds the greatest brightness within the image. This peak value, times a process gain coefficient is placed in a peak map. The original image is reduced with the same value times a normalized dirty beam, or Point Spread Function (PSF), and with this new image the process is repeated all over again. When a certain brightness level, noise determined, is left in the processed image, the process is stopped. The resulting peak map is convolved with an ideal beam, or PSF, and with remaining noise added it is presented as the final cleaned map.

There are versions of CLEAN for the coherent case that takes care of the fact that the beam is a complex function with an associated complex phase [50]. This causes different brightness sources to interfere with each other when they are also at some distance apart. When the interference is constructive false brightness peaks appear, and when the interference is destructive you get false dark zones. This phenomenon is also known as speckle. The dirty map then may contain zones with only noise energy. By identifying several peaks in the same map, and testing them in a tree structure it is possible to eliminate some of the false brightness peaks. Each node in the tree corresponds to a possible image and path towards a final cleaned image. The nodes with least amount of image energy are supposed to be the most probable path towards a correct final peak map. A large number of nodes at each process level increase the complexity, but also facilitates an increased process gain and a faster convergence.

The MEM method uses the information entropy definition. It tries to fit a map that both satisfies the measured data and at the same time gives the

highest entropy. If we consider high entropy as measure of high degree of information content, then this map is the map that contains most information and still satisfies the measurement. Since noise is highly unpredictable it is said to contain much information, consequently a map with high entropy is very noisy. The allowed noise content is given by the estimated noise in the measurements. Another useful constraint is the total flux or received power. The map must not contain more energy than the actual measurement. This could however be violated in the case of coherent measurement where speckle may occur.

Superresolution is defined as the ability to resolve spatial frequencies outside the spatial bandwidth of the imaging system [47]. Superresolution is possible under certain conditions. The true image has to be nearly black. If n is the number of samples and m is the number nonzero components in the Fourier transform of the PSF, $\epsilon = m/n$ is the incompleteness ratio. If the true image is $\frac{1}{2}\epsilon$-black the image has to admit superresolution. If the true image is not ϵ-black the image cannot admit superresolution. Superresolution is often admitted in the case of astronomical images, where the true image consists of distributed point-like sources.

3.2 Description of experimental radar interferometer

The complete experimental interferometer consisted of a patch antenna array, a cable harness, a switch matrix, microwave- and control-electronics, and a back end PC, Fig. 3.3. The patch antenna array was covered by a ceramic window and mounted in a dedicated protecting steel tube cooled with nitrogen. The antenna array elements were accessed with a switching network. A single patch was dedicated for the illumination of the burden surface [51]. The use of a single transmitting antenna simplifies the realization of the interferometer, but with this simplification we loose some of the achievable resolution. This is a consequence of the geometric time delay, τ_g in Fig. 3.1, being accounted for only once, namely on the signal reception.

The environment where the interferometer was situated is very demanding. Hot gases are continuously flowing upwards and dusty materials are charged from the top. There is normally an overpressure with smaller variations inside the blast furnace. Dust obscure the sight for optical instruments and deposit on surfaces. The temperature may vary during the process cycle, stressing the mechanical structures. During maintenance stop the temperature can fall down to the ambient outdoor temperature, while during production it may peak at several hundred degrees of Celsius. The atmosphere inside the furnace contains water vapor, which may react with other chemical components and form, for instance, hydrochloric acid(HCl). If there is an accretion formation of material on the inside of the furnace wall, or if a vault or cave is created, the blast furnace operation is affected in a negative way. It then may be necessary to sprinkle water on the burden surface. The raw material absorbs this water and the increased weight eventually causes the stuck material to cave in. Besides an increase of water vapor content and possibly a sudden change of pressure, ballistic projectiles of raw material may hit the interferometric sensor.

The given preliminary requirements for the interferometer are displayed in

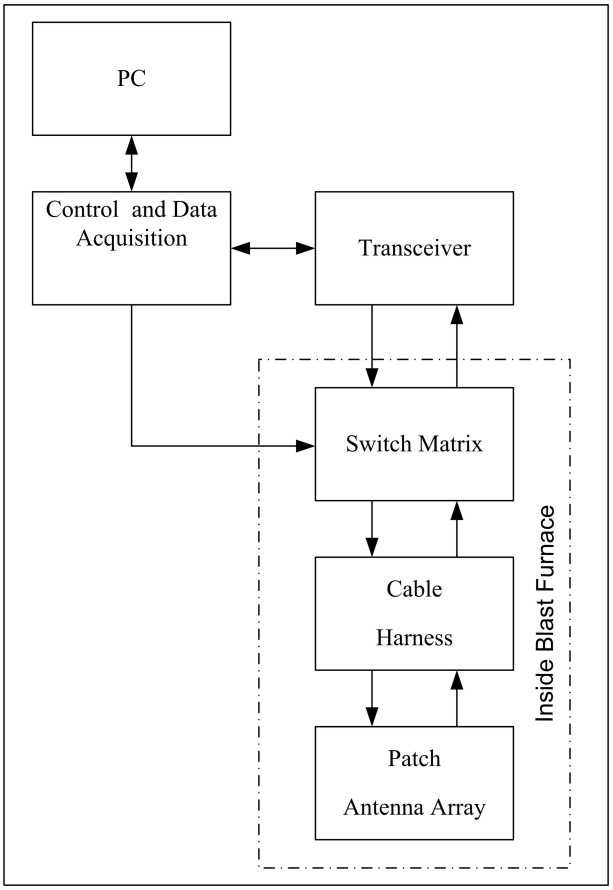

Figure 3.3: *Block schematics of radar interferometer.*

Table 3.1.

Table 3.1: *Preliminary requirements for the interferometer.*

Performance Req.	*Typ*	*Min*	*Max*	*Unit*	*Remark*
Measurement speed:					
Shutter time			30	s	
Processing time			240	s	
Sensor parameters:					
Frequency	11	5	22	GHz	*Allowed*
Range	5000	2000	7000	mm	*Required*
Illumination angle	120	90		^{o}	*Required*
Angular resolution	10			^{o}	
Range resolution	250			mm	
Dimensions:					
Diameter	200			mm	*Circular cross section*
Height	1000			mm	

Environment Req.	*Typ*	*Min*	*Max*	*Unit*	
Temperature:					
Ambient	400	-20	700	^{o}C	*Required*
Radiation			1200	K	
Atmosphere:	CO, CO_2, H_2, H_2O, SO_2, HCl and electrically conductive dust				

The requirements on shutter and processing time emanate from the assumption of a stationary target and the minimum response time for a meaningful process control. Typical blast furnace sizes give the needed illumination pattern and resolution.

3.2.1 Signal system

The radar interferometer illuminates the target, consisting of reflective surface elements, with continuous electromagnetic waves that are stepped through N_ω discrete frequency channels with a free space wavelength centered around λ_0. Here the target is modelled as a spatially discrete apparent brightness distribution vector $\boldsymbol{B}$, associated with a vector $\boldsymbol{r} = \hat{\boldsymbol{r}}|\boldsymbol{r}|$ of three dimensional spatial coordinates with its origin in the interferometer imaging reference point. We also assign a vector $\boldsymbol{r_{TX}}$ of spatially coordinates with its origin in the transmitter antenna position. The coordinate vectors elements are numbered by the index variable i.

By sampling the reflected returning wavefront at coordinates on a uv-plane corresponding to different baseline lengths measured in number of wavelengths, and orientations in a vector $\boldsymbol{u}$, here numbered by the index variable k, a vector $\boldsymbol{\mathcal{V}}$ of complex amplitudes of the spatial angular frequencies are measured. The index variable k represents the base lines made up by the combination of antenna element indexed by m and n.

A basic principle in antenna theory is the reciprocity relation between receiving and transmitting antennas [52]. It states that by analyzing transmitting

antennas we get the properties of receiving antennas as well. If we consider the antenna to be in the origin of a spherical coordinate system, $\boldsymbol{r} = (r, \theta, \phi)$, and if r is sufficiently large, then the radiated electric- and magnetic-field components are perpendicular to the vector $\boldsymbol{r}$. This is the same as the far-field or Fraunhofer approximation being valid. The antenna pattern can now be stated as an r independent function $F(\theta, \phi)$, commonly normalized to a maximum value of one. The far-field approximation starts to hold at a radial distance greater than,

$$R_{\text{ff}} \gg \frac{D^2}{\lambda_0}, \tag{3.17}$$

where D is the diameter of the antenna. The half-power beamwidth is defined as the angular width of the main lobe between the two angles at which the magnitude of the antenna pattern, $F(\theta, \phi)$, is equal to half of its peak value.

The directivity $D(\theta, \phi)$ of an antenna in a direction is the ratio of its normalized radiation pattern $F(\theta, \phi)$ in that direction, to its average over the complete sphere. The maximum directivity D_0 of an antenna is related to an effective area A_e of the antenna,

$$D_0 = \frac{4\pi}{\lambda_0^2} A_e = \frac{4\pi}{\lambda_0^2} \eta_a A_p, \tag{3.18}$$

η_a is the aperture efficiency and A_p is the physical aperture of the antenna.

The efficiency factor η_a in (3.18) may also include ohmic losses and matching losses. The matching losses result in signal energy being reflected back to the source. The energy is, if reflected back into the transmitter, lost in the source impedance. If the received energy is reflected back into the antenna, it will be retransmitted. In both cases it contributes to a lower signal level and a higher noise level. The mismatch energy may screen real targets or may be interpreted as a false target in a radar.

The effective aperture area A_e is important in the definition of the Friis transmission formula that relates transmitted power, P_t, to received power , P_r, in a transmission system. With a distance R between transmitter and receiver we get

$$P_r = \frac{P_t}{4\pi R^2} G_t A_e = S A_e, \tag{3.19}$$

where the available power density, S, is intercepted by the effective collecting antenna area.

The resolution of the interferometer is determined by microwave frequency bandwidth, microwave center frequency and the size of the interferometer aperture. The resolving power in radial direction is determined by microwave frequency bandwidth as in (3.2),

$$\Delta r = 0.443 \frac{c_0}{f_{\text{BW}}}. \tag{3.20}$$

The angular resolutions are determined by the uniformly weighted interferometer with the size D as,

$$\Delta\theta_{nadir} \simeq 0.886 \frac{\lambda_0}{D}, \tag{3.21}$$

and individual antenna element distribution function respectively. For other looking angles than nadir, we have to compute the angular resolution with a projected aperture diameter as,

$$\Delta\theta \simeq 0.886\frac{\lambda_0}{D\cos(\theta)}. \tag{3.22}$$

In a cartesian coordinate system the radial and angular resolutions will become combined and quite difficult to define. Around a position $\boldsymbol{r}_i = (r_i, \theta_i, \phi_i)$ the resolution in cartesian coordinates may be approximated with,

$$\Delta x \simeq \Delta r \sin\theta_i + r_i \Delta\theta \cos\theta_i \tag{3.23}$$

$$\Delta y \simeq \Delta x \tag{3.24}$$

$$\Delta z \simeq \Delta r \cos\theta_i + r_i \Delta\theta \sin\theta_i. \tag{3.25}$$

The sensitivity of the interferometer is determined by the noise, gain and intermodulation budget of each antenna element receiver chain. Since the interferometer system transmits a CW signal at a low level of power, intermodulation is considered a non critical part of the system budget. A key parameter in any radio system for radar or communication purposes is the signal to noise ratio defined as,

$$\mathrm{SNR} = \frac{P_r}{P_n}, \tag{3.26}$$

where P_n is the noise from the receiving system. The receiver noise is determined by the system parameters, noise bandwidth, f_{LF}, and system temperature, T_{SYS} or noise factor, F_{SYS}. We have,

$$P_n = kT_{\mathrm{SYS}}f_{\mathrm{LF}} = kT_0F_{\mathrm{SYS}}f_{\mathrm{LF}}, \tag{3.27}$$

where k is the Boltzmann constant. With a definition of SNR that includes radar cross section, σ as,

$$\mathrm{SNR} = \frac{P_tG^2\lambda_0^2\sigma}{(4\pi)^3R^4P_n} \tag{3.28}$$

a minimum detectable Radar Cross Section (RCS) for a given minimum acceptable SNR can be calculated.

Phase errors and generation of the transmitted signal

Phase errors can be divided into two parts, random phase error (phase noise) and deterministic phase errors [43].

The phase noise of the signal limits the ability to focus the image. A stable and well controlled transmitter frequency is generated by use of phase locked loops (PLL). The maximum possible rate of the frequency sweep is set by the phase noise requirements which in turn limits the shutter speed of the system. A fast frequency sweep requires a fast lock-in time as the output frequency is swept in steps. With a wide loop bandwidth we get a rapid response at the cost of an increase in phase noise.

Minimum frequency step size is determined by the reference signal frequency and the phase noise requirements of the PLL. Phase noise performance inside the

loop bandwidth is governed by the reference signal. A small step size requires a low reference frequency, but the multiplication factor N needed to achieve the output frequency then is increased. Consequently also the output phase noise power, which is the reference phase noise power increased with $20 \log N$ in dB, is increased.

Different regions of offset frequencies for the phase noise, f_{offset}, can be identified. They are determined by the measurement range of the radar, or radar interferometer, and by the rate of the frequency sweep.

- Very short term phase drift, within duration of one frequency sample ($f_{\text{offset}} > 1000$ Hz), reduce the receiver sensitivity.
- Short term phase drift, within one frequency sweep (5 Hz $< f_{\text{offset}} <$ 1000 Hz), reduce the ability to compress the synthetic range pulse.
- Long term phase drift within one scan of the antenna ((1/30) Hz $< f_{\text{offset}} <$ 5 Hz), reduce the ability to compile the interferometric image in cases of sequential baseline scans.
- Very long term phase drift limits the lifetime for the calibration measurements ($f_{\text{offset}} <$ (1/30) Hz).

Deterministic phase errors also effect the PSF of the system. These phase errors can be characterized by the group delay, or dispersion of the system. A signal phase shift that varies linearly with frequency gives a flat group delay. Narrow-band resonant structures as sharp filters show a nonlinear phase response, often sensitive to temperature variations. The use of bad calibration data is another source of deterministic phase errors. A simple classification of deterministic phase errors and their impact are listed below.

- Linear phase errors cause a spatial shift of the focused image.
- Quadratic errors cause a symmetric widening of the PSF, decreasing resolution.
- Cubic errors cause unsymmetrical distortion of the PSF, decreasing resolution.

3.2.2 Interferometer array design

The actual sensor consists of an array of small antenna elements. Since we sample a finite aperture at a limited number of points, sidelobes occur, resulting in a so called dirty beam. Reduction of sidelobe energy can be performed by a weighting value w_k for each baseline, but this reduces the effective aperture size and thus the angular resolution. The dirty image with weighting function becomes,

$$d_i(\tau_r) = \sum_k w_k \mathcal{V}_k(\tau_r) \exp(-j2\pi \boldsymbol{u}_k \cdot \hat{\boldsymbol{r}}_i), \tag{3.29}$$

where $\boldsymbol{u}_k$ are the coordinates on the uv-plane corresponding to the baselines being sampled, $\mathcal{V}_k$ are the visibility functions from cross correlation of antenna voltages, $\hat{\boldsymbol{r}}_i$ is unit position vector, and τ_r is the delay time corresponding to

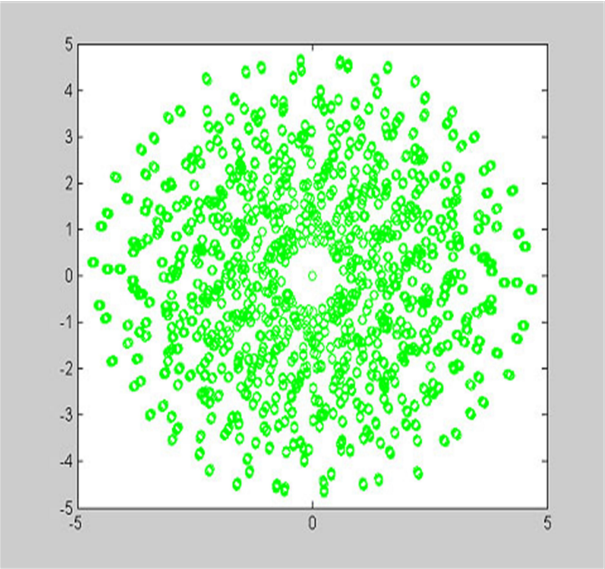

Figure 3.4: *Baselines of the interferometer plotted on the uv-plane (in wave length units). This plot shows the so called UV coverage of the interferometer. The lack of short baselines is a consequence of antenna isolation requirements prohibiting antenna elements to be placed close to each other.*

different radial distance from the interferometer. This gives a data set of radially stacked two dimensional images in a non-Euclidian angular coordinate system, further described in [51]. Transformation to other coordinate systems can be performed by a resampling procedure.

A second order error causing abberation will be introduced since we assume planar wavefronts and a small antenna, i.e. Fraunhofer diffraction. The far-field distance R_{ff} where the Fraunhofer approximation starts to hold is given by,

$$R_{\text{ff}} \gg \frac{D^2}{\lambda_0} \simeq \max_k |\boldsymbol{u}_k|^2 \lambda_0, \tag{3.30}$$

where we used that ($D \simeq \max_k |\boldsymbol{u}_k| \lambda_0$). For our interferometer the far-field approximation is valid for distances greater than 849 mm. In the blast furnace the interferometer is situated three to four meters above the burden surface. The usable field of view for the interferometer is set by the individual antenna element opening angle. Requirements from the application set this parameter to at least 90 degrees. The maximum measurable field of view with the interferometer is determined by the requirement that geometrical time delay in Fig.3.1, τ_g, should be less than f_{LF}^{-1}. This, however, is of no concern in our case since the maximum baseline length covers only a few wavelengths and the stepped frequency method gives us an instantaneous bandwidth, f_{LF}, of a few tenths of kHz. Further, the coherence time of the used signal source is far greater than τ_g.

The angular resolution, or half-power beam width, in radians, of a two element interferometer is determined by the wavelength of the radiation and the

length of the baseline D_λ, see Fig. 3.1, spanned by the antenna elements [53],

$$\theta = \frac{1}{2|D_\lambda|}. \tag{3.31}$$

Compared to the uniformly illuminated circular aperture this is an improved resolution by a factor of 2. In the current application a resolution of about 10 degrees has been considered to be sufficient, see Tab. 3.1. With $\lambda_0 \simeq 27\ mm$ and a interferometer diameter of 150 mm, we are well within the required resolution. The effective interferometer solid beam width Ω_b is set by the baseline coverage in two dimensions, and the illumination, or weighting, function used. Note that all surface elements dA_i within the solid beam width Ω_b are summed to produce the received brightness in each angular pixel. The number of such surface elements scale as r_i^2, the brightness from each fixed surface element scales as r_i^{-2}. The brightness received by the interferometer system per beam solid angle therefore is independent of the distance. The illumination of each surface element is dependent on the distance to the transmitter r_{TX}^{-2}. The brightness per resolution pixel received by the radar interferometer signal is therefore proportional to r_{TX}^{-2}. Radial full width at half power, Δr, of the synthesized pulse is according to (3.2),

$$\Delta r = 0.443 \frac{c_0}{f_{\mathrm{BW}}}. \tag{3.32}$$

In our case the bandwidth is $f_{\mathrm{BW}} = 600$ MHz giving a $\Delta r \simeq 220\ mm$. The number of baselines in an interferometer is [46],

$$M = \frac{N(N-1)}{2}, \tag{3.33}$$

where N is the number of physical antenna elements. It would be preferred if each baseline gave a unique sample of the uv-plane since redundant baselines add no new structural information about the target, assuming a completely incoherent surface brightness. Redundant samples merely increase the signal to noise ratio. Although some methods [54] are proposed for minimum redundancy in distribution of the antennas, it is also known that, if N is large enough, it is sufficient to spread them out in a random fashion, as in this work. The coverage of the uv-plane of the interferometer is shown in Fig. 3.4

Making the antenna elements small compared to the free space wavelength makes it possible to both map a wide field of view and fitting a large number of antennas inside the perimeter of the interferometer. A drawback of smaller antenna elements is the reduced antenna collecting area, resulting in a lower SNR value. The choice of a planar antenna array gives a mechanical stable and accurate positioning of each element and an unsensitive surface. Antenna terminals are preferably placed on opposite side of the array than the patches, making the substrate surface less crowded and minimizing spurious radiation. A quadratic patch with circular polarization was designed. The use of circular polarization makes it possible to rotate each antenna element in the plane of the array, allowing an easier fit and positioning of the elements. The constant phase error introduced by this rotation is compensated by a unitary complex coefficient in the Fourier transform. A cross-section of the circuit substrate topology is shown in Fig. 3.6. When a combination of small size antenna element and low

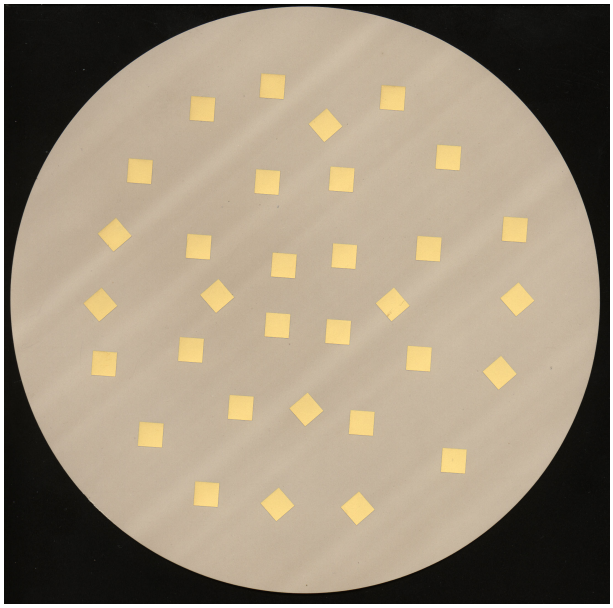

Figure 3.5: *Photo of the front of the patch antenna array showing antenna elements (patches).*

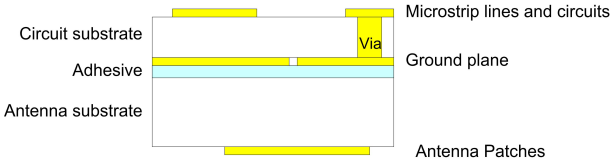

Figure 3.6: *Subsection of part of the antenna array showing substrates and metallic layers making up circuits and antenna elements (patches).*

radiating resistance is wanted, conflicting requirements on dielectric constant of the antenna substrate are raised. A compromise between size of patches and radiation impedance was met by a using Duroid 3003, a substrate with a dielectric constant of $\varepsilon_r = 3.0$. A low dielectric constant also reduce surface waves causing cross coupling between antenna elements [55]. Fig. 3.5 show the front of the final antenna array.

An aperture coupled, or slot coupled, patch antenna was considered to fulfil both the requirements of easy planar fabrication and sufficient bandwidth. This method of coupling gives lower back radiation and the freedom to have different substrate thickness for circuitry and patches. A thicker antenna substrate gives a more efficient radiating patch, while a thinner substrate for the circuitry reduce the back radiation [56]. Further, the patch covers the coupling aperture, reducing parasitic radiation from the ground plane slot. The slots are excited by transmission lines feeded by a hybrid circuit.

The complete interferometer was integrated with a computer controlled switch matrix and semirigid coaxial cables fitted with coaxial push on connectors. The push on connectors makes it mechanically possible to mount a very dense microwave harness. Unwanted radiation from microstrip transmission lines is minimized with this configuration, since all microstrip lines are very short and covered by the ground plane.

3.3 Results and discussion

The results presented here are from simulations with single and multiple discrete targets and from measurements. The interferometer functionality was verified by measurements on single antenna elements and on a complete interferometer setup. A microwave vector network analyzer was used for the measurements in both cases. A coaxial switch matrix was used to scan through the available interferometry data, assuming a steady state target surface. Simulated measurement data from an interferometer was generated by a ray tracing algorithm, and processed by a domain transforming algorithm. The same domain transforming algorithm, transferring data from spatial frequency domain to spatial delay domain, was used for the measured data. A third algorithm was used for presentation of the images. Yet other algorithms were made for testing CLEAN.

The patch antenna array was covered by a ceramic window and mounted in a dedicated protecting steel tube cooled with a continuous flow of nitrogen.

The simplest output data, except for cold sky noise measurement, is the response from a single scattering point target, see Fig. 3.7. Simulation of a single target was used to obtain the point spread function(PSF) of the system at different ranges and positions. Later these simulation could be used to verify the actual measured PSF of the patch antenna array. The PSF is determined by the bandwidth, (3.2), and the antenna array configuration.

The imaging possibility was tested by moving an active point source around on the laboratory floor. This verified the coordinate system and also that we were able to find the position of a reflector in all three space coordinates. The active point source consisted of a wide opening angle antenna connected to the transmitter output of the interferometer through a flexible coaxial cable. The active point source was later replaced with a passive metallic reflector made out of copper, see Fig. 3.8. With this setup the crosstalk in the array was

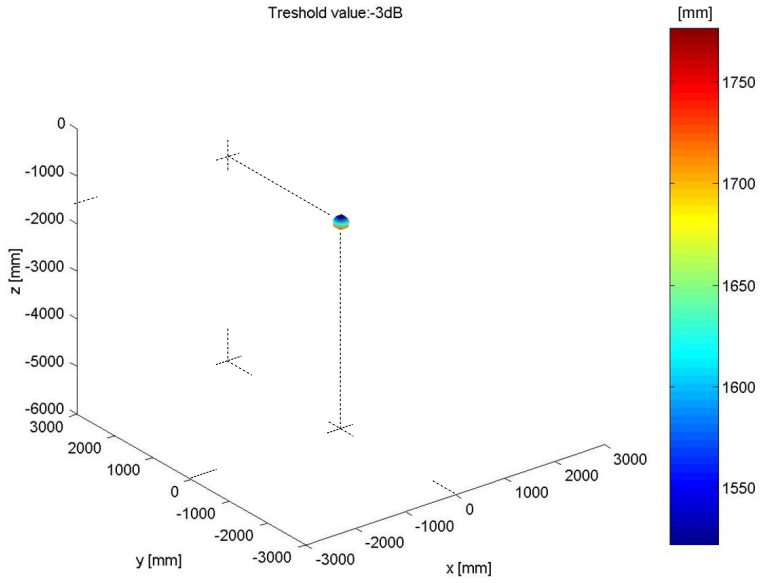

Figure 3.7: *Example of simulated response from a point scatterer 1600 mm below the origin of the interferometer. The object in the image is delimited by a surface generated by connecting the points in the space where the intensity of the response has fallen to half of its maximum. Distance from interferometer origin is coded by color. The radial half-power limits of the response, extends from approximately 1525 mm to 1775 mm, which gives a radial resolution of 250 mm.*

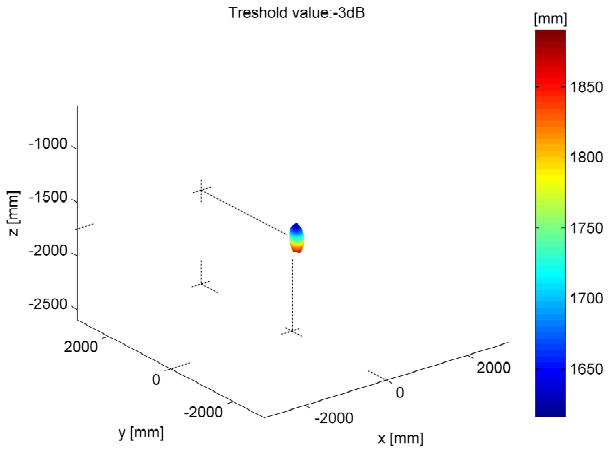

Figure 3.8: *Detection of reflection from Cu-mirror with a dimension of (*40x40cm^2*) and placed 1750 mm below the interferometer origin.*

Figure 3.9: *The laboratory imaging experiment setup, in this case with coke spread on the floor. The interferometer array is found at the top center of the image.*

detected and could be spatially filtered by rejecting the response from the first few decimeters of the interferometer.

A layer of coke formed a surface on the floor of the laboratory. The surface was manually altered and measurements were taken between each alteration, see Fig. 3.9. Differential images made by subtracting the datasets displayed a sensitivity to these surface changes, Fig. 3.10. The measured result may be compared with the simulation in Fig. 3.11. Imperfections in the beam can be seen together with sidelobes in the measurements. The sensitivity was improved by moving the transmitter antenna, from within the array to an external position, thus reducing crosstalk.

The actual reconstruction of the surface is quite difficult and was underestimated in this project. By introducing several point targets in simulations, the speckle phenomenon was studied and an approximation of a surface could be made. A ray-tracing maximum intensity algorithm proved to be insufficient. Speckle and sidelobes causing false detections make this approach impossible even in an ideal case. The maximum intensity algorithm detects the response from the closest scatterer, which will dominate over more distant scatterers,

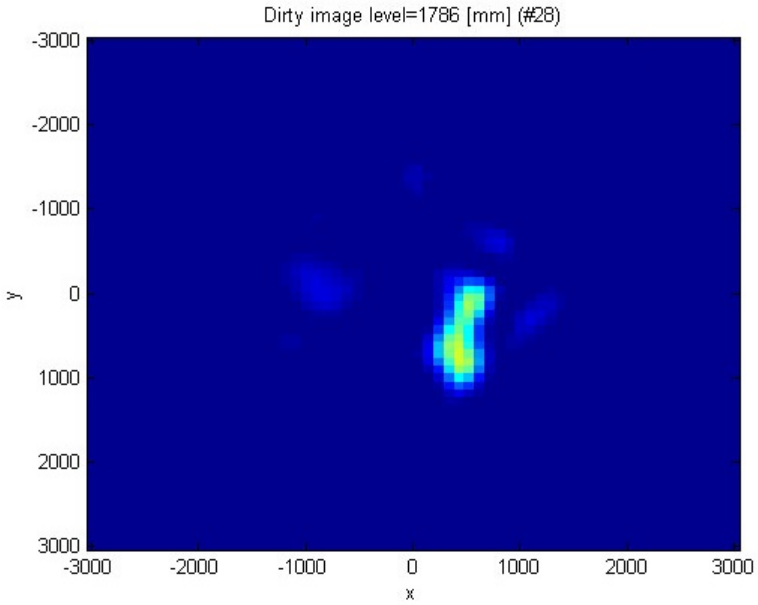

Figure 3.10: *Example of measured reflection at radial distance 1786 mm coming from alterations made on the coke surface in Fig 3.9. Intensity is here normalized and coded by color. The unit of the axes is mm.*

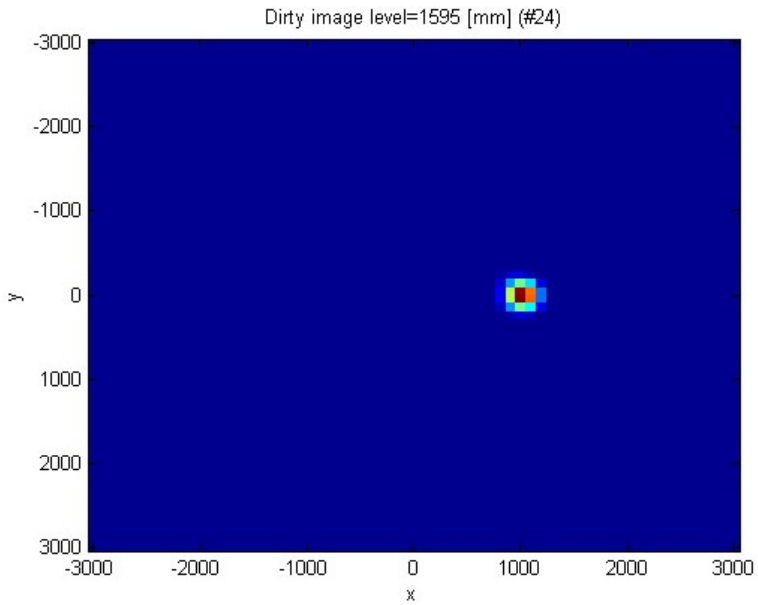

Figure 3.11: *Simulated reflection from changes in a reflecting surface 1600 mm below and 1000 mm offset from the phase-center of the interferometer. Intensity is normalized and coded by color. The unit of axes is mm.*

and instead of the correct plane surface a bowled topography will be the output. Further, in an implemented interferometer the crosstalk between antenna elements will screen the real surface reflections and cause false response. An initial attempt to use the CLEAN algorithm gave a promising response but had a too long processing time, and the most distant and faint objects could not be properly detected, see Fig. 3.12. The CLEAN algorithm gave less false detections than the maximum intensity algorithm. A faster algorithm can be obtained, but it will still rest on the approximation of a limited number of discrete point scatterers.

During the project we assumed a connected surface, but still there are difficulties with hidden and shadowed regions that must be solved. Further, dark zones may be created by several mechanisms, such as specular reflections directed away from the sensor, by lossy material, by depolarization or by speckle, or by sidelobes from close scatterers interfering destructively and cause dark zones.Using historical data of the surface topography is a good way to disqualify improbable solutions, such as sudden steps in height or tilting angle of the surface. Thus, the final surface model must include a multitude of parameters, such as speckle, specular reflection, surface roughness and scales, shadowing, sidelobes, depolarization, spatial history and history in time.

The experiments show that the radar interferometer is sensitive to surface alterations, and that it may be assembled from relatively low cost components. For its utilization in industrial process control the signal processing has to be further developed and the protective encapsulation has to be improved. Radio astronomy signal processing methods have often shown to be inappropriate for radar interferometry due to the spatial coherency of the source.

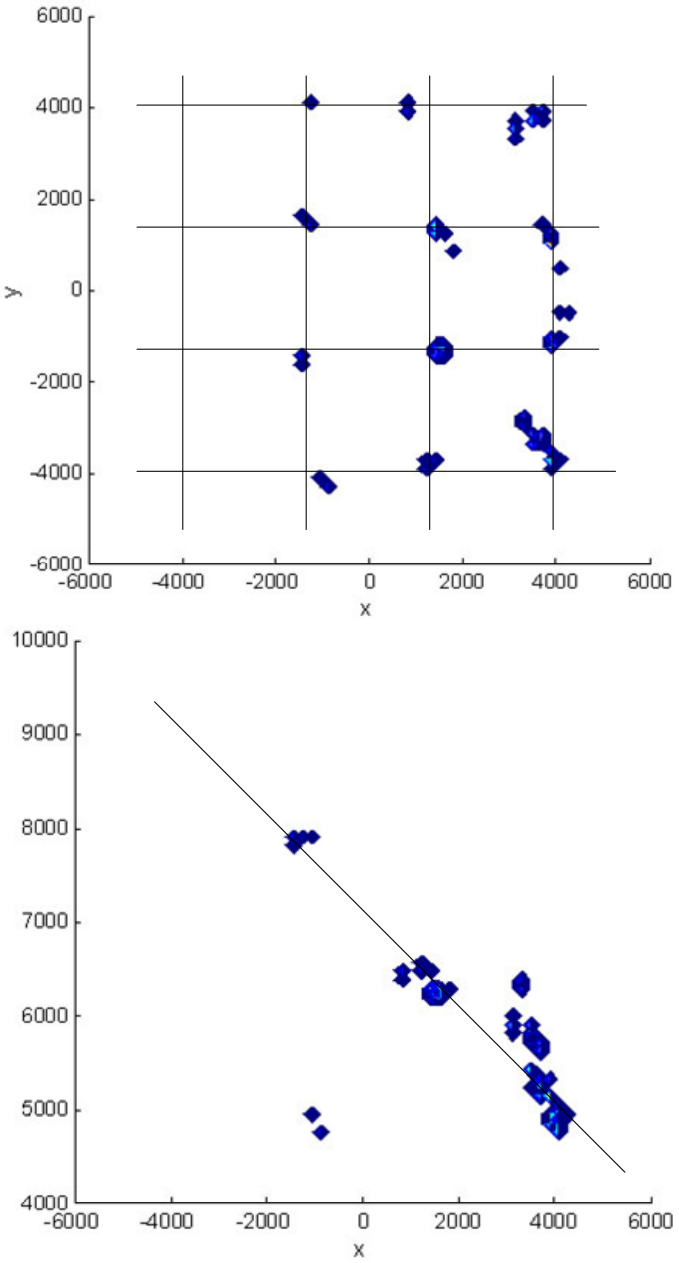

Figure 3.12: *CLEAN algorithm output from simulation of 16 scatterers evenly distributed on a slanting plane, in xy- and xz-plane. The correct position of the scatterers are indicated by the crossings of the help grid lines. Note that the z-axis is reversed compared to other images. Unit of axes is mm.*

Chapter 4

Conclusion and outlook

4.1 Conclusion

Low power solutions have become increasingly important for electronic design [7], and low power radio can be achieved when power is prioritized already in the system design phase. On-chip integration of radio electronics is part of the solution, but it also bring new difficulties to address.

The most interesting technology platform for low cost radio nodes is the CMOS process. CMOS process development is mainly driven by the requirements of digital electronics, and radio designers have to adopt accordingly. The upside of the ongoing reduction of linewidths is the increase of available transition frequency f_t of transistors, which is beneficial for the RF designer. However, along with the reduced transistor size comes an increased sensitivity to over-voltage, where the gate oxide is the most sensitive part. It takes only a few volts over the gate oxide to damage the insulation. Addition of on-chip ESD protection circuitry to counteract over-voltage comes at a cost of added parasitic loads. These parasitic elements have to be be taken into account when designing the RF front end.

In some cases the ESD protection circuitry will be the limiting factor of performance, leading to a complicated trade-off between performance and level of protection. Further there is a reluctance to add any external components when adding new functionality to an ASIC. This goes also for wake-up functionality, which ideally should be implemented as an IP-block to any general ASIC. This basically restricts the technologies available for implementation of WuRs to ordinary CMOS processes.

The ever increasing use of electronic equipment in general, and radio equipment specifically, increase the levels of EM-interference. The situation is complex without a good overall picture of the existing interference environment. For many systems the sensitivity analysis is dominated by interference rather than the thermal noise. This problem must be addressed by both MAC protocol innovations and by hardware innovations (regulative work must also take the new situation into account). New tools for analysis are needed for efficient trade offs in the system design phase.

Efficient MAC protocols are needed for better spectrum efficiency [29][26]. The synchronization in the protocols depend on accurate timing and/or accurate

frequency control [57][58]. Inaccuracy in frequency will force MAC designers to insert larger guard bands reducing the spectrum efficiency. Drift in time results in longer awake time for duty cycled receivers causing increased energy consumption. Accuracy in time and frequency require well performing resonators or delay lines. A good resonator should be stable and independent of environment variables as temperature and vibration. While low loss resonators tend to be bulky and expensive, stability can be reached by arrangements like ovens or compensating and controlling electronics, at the cost of power and component count. Lossy resonators need to be compensated with active amplifiers to form oscillators, but still they exhibit phase noise due to their losses. This implies that precision in time and frequency is unachievable in applications requiring both low power and small sized radio nodes.

Key components are resonant tanks and reactive loads needed for oscillators, filters, transformers, and amplifiers. Well performing reactive components are difficult to minimize and/or to integrate. Integrated on-chip inductors offer low Q-value and occupy large and costly silicon area. Therefore on-chip inductors are costly and not very attractive in solutions for tank circuits. Using lower grade resonators mean higher loss and therefore a need to compensate with higher gain which in turn leads to increased power consumption. Further, the effect of losses can not be totaly overcome by active components, noise, phase noise and jitter will still be the result. With higher carrier frequencies the use of distributed components on substrate can offer a reduced component cost, but this requires stable and good quality substrates; for moderate frequencies FR4 has proven to perform quite well. High quality substrate materials with low loss are expensive and have relatively low dielectric constants, this leads to tank circuits occupying fairly large areas.

At lower frequencies active inductors is an alternative although they are inherently more noisy than their passive counterparts. Finally, an interesting and a bit surprising result from this work is that resistive loads are competitive with passive and active inductors as output load for integrated amplifiers even at radio frequencies.

Microwaves have the ability to both sense and carry information over distance. The integration of microwave and digital electronics enable sensor applications requiring heavy computational resources at low power and low cost, such as imaging interferometers or similar antenna arrays. This heavy integration is now possible even at mm-Wave frequencies [59], but the volumes are often to small to justify the cost [60].

4.2 Outlook

Wireless Sensor Networks (WSN) is a kind of synthesis of sensors and RFID. In a larger perspective these sensor networks are the elements that become the Internet of Things (IoT), which is visioned to create wisdom out of data as in Fig. 4.1.

IoT has been sketched as a three layered architecture, see Fig. 4.2, with powerful computing and data storage facilities in the innermost core, and with a swarm of sensors all around us in the outmost layer of the architecture [61]. In between, hand held devices will mediate the information and present the stored and processed data from the core. This communication between layers

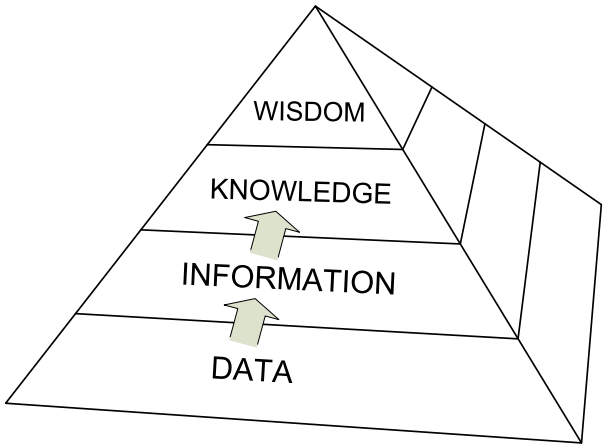

Figure 4.1: *A vision of how data is transformed to wisdom by the Internet of Things (IoT). Data is collected from sensors and transferred and processed by ubiquitous low power electronics.*

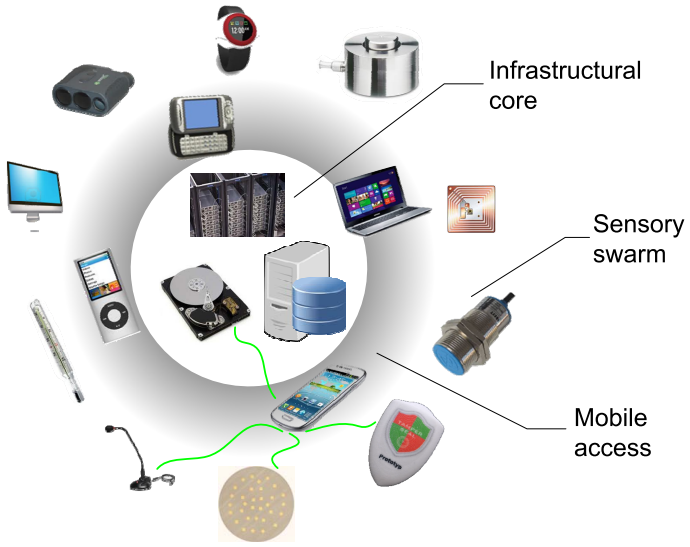

Figure 4.2: *A vision of how IoT is made up of different structural layers [61]. Radio will be used for communication between layers, while remote sensing will be used in the outmost layer.*

needs to be wireless, with a high degree of flexibility and a good coverage, and is predicted to essentially be one of the most challenging details of the system to realize [7]. Microwaves will be used for communication and sensing at all levels. However, there are wide variation in the requirements. While the communication between the innermost core and the middle layer may require data rates of 100 Mbps and very low latencies (<1ms) everywhere, the communication between the sensors and the middle layer may be measured in kbits per second and with an undetermined latency period. In the latter case the most important building block from a power perspective in the wireless communication chain is the receiver of the sensor rather than the transmitter. This is a result of long inactivity periods, where transmitters are asleep but the receivers have to always be awake.

IoT, Ubiquitous Computing, and Pervasive Computing are all terms with a similar meaning, describing a widespread occurrence of radio nodes in our everyday life. The nodes may perform simple tasks and between uptime have long periods of inactivity. They must be small, cheap, and functional for several years without need for service. Improved logistics, tracking of goods, transportation management, and sensing are some of the motivational factors behind the development. This has pushed the RFID technology forward, and the need for large numbers of nodes requires extremely low cost solutions.

As the IoT is expected to be a part of our everyday life and incorporated in critical systems such as medical devices and transport systems its robustness is vital. The constituting nodes has to withstand environmental factors such as temperature, moist, shock, vibrations, and a very dynamic and changing electromagnetic situation.

The described requirements of small size, low power consumption, robustness, and low unit cost, are very demanding. These issues can only be solved if one considers the total system, with its radio nodes, readers, back end systems, software, hardware, and protocols as a whole. Thus a close collaboration between designers at different layers and a focus on application is necessary. Application focused design may however result in very heterogenous solutions being difficult to merge with other systems.

The size of each node is many times set by the battery and the antenna. New antenna designs are needed that better make use of the total volume available for the node instead of being two-dimensions structures only. Prediction of the antenna coupling to the environment is difficult for mobile devices and further requires comprehensive simulations throughout the design phase. Batteries must not only be dimensioned to supply the average power needed, but also the peak powers developing during start up and at transmission bursts.

Energy scavenging technology is improving making it possible to counteract the battery drain or to remove batteries completely. Energy scavenging make use of vibrations, light, thermal energy, and electromagnetic smog. Ability to store energy in super capacitors and batteries make such solutions more robust. These otherwise unreliable and unstable energy sources call for ways to evaluate quality and stability and possibly to dynamically modulate the load [62]. Supplying energy over the air with the RF-signal is today commonly used in RFID technology and offer good system control over the energy source. Research is here made to improve RF-DC conversion and to lower radio power consumption on the chip, but efforts are also made by investigating power optimized waveforms having higher peak to average power ratios [63].

New materials and processes result in new components for high speed electronics. Examples are graphene transistors and wrapped gate transistors [64]. MEMS technology offer new low loss resonators; Bulk Acoustic Wave (BAW) filters are used for pre-selective filter at radio frequencies [15]. Battery technology is improving with higher energy densities, being exploited to make radio nodes smaller and live longer. Flexible solutions with printed batteries offer modest energy density and low peak power, but also the possibility to tailor the battery size and form factor. Mechanically flexible battery materials must be developed to ensure new and ductile form factors. A designer further wants flexibility in her choice of battery capacity so she can optimize the lifetime of the radio node.

Moores law still holds and we may expect digital electronics to push line widths to be smaller, enabling high speed transistors possible to use in subthreshold regime for radio electronics. The cost per radio node is reduced as silicon footprint is reduced, and more functionality may be integrated. This is true as long as many identical units can be fabricated. For low volume production there are possibilities to use FPGA, and a growing availability of programmable radio ASICs off the shelf. Miniaturization may be an issue with such solutions, but as discussed earlier, batteries and antennas are the largest components. The increased computation capabilities with digital electronics can be used for built in self test (BIST) methods and in-vivo calibration. This may e.g. be used to dynamically compensate antenna mismatch due to changing electromagnetic environment of the radio [9] or to overcome spread in material parameters. BIST further provides tuning possibility of poor frequency and time reference oscillators. MAC protocols may include processes for periodical tuning of the nodes to a common reader reference [31]. Massive MIMO is yet another microwave application made possible with improved computational capacity.

Old analog wireless services are closed and frequency bands are freed up that may host smarter digital applications. The use of higher carrier frequencies is exploited for higher data rates, to escape to quieter frequency bands and limiting the interfering range (60 GHz). Higher carrier frequencies further enable miniaturization of antennas and for beam forming with reasonable sized arrays. Higher frequencies take on more sophisticated production methods, often expensive, and the use of new unproven materials or production methods to meet performance.

Radio communication has for a long time focused on providing larger bandwidth with higher data rates. This has lead to the use of increased carrier frequencies, higher density of radio cells and shorter communication ranges (e.g. 60 GHz WLAN). However, today in many radio applications (e.g. military, leisure, and sport) there must be an increased awareness of the radio environment and of the user behavior. Such new intelligent radio systems form ad hoc networks, and instead provide the bandwidth or range needed for the situation.

Modern radio systems are in many cases limited by interference rather than by thermal noise. New methods and components have to be developed to help system designers in their work. An example is multiband radio frontends that could be realized with generic wideband Software Defined Radio (SDR). Such a receiver solution could replace several separate hardware receiver blocks, minimize cost and maintain flexibility. However, the receiver is consequently exposed to a wide spectrum of interfering signals. The required dynamic range of the receiver to be handled is set by the level of interference. The required dynamic range of the receiver, and thereby the power consumption, could effectively be

reduced by filtering out out-of-band interfering signals in a preselecting filter. However, today there is no good solution for such an interference managing preselecting filter with low power consumption, high dynamic range, small size, being electronically controllable over a wide bandwidth.

From being rare and sometimes referred to as black magic, microwave technology has become omnipresent in, and essential for, the vision of ubiquitous computing and IoT. Further, considering the development of power consumption, there is obviously plenty of room at the bottom.

References

[1] E. Nilsson and L. Baath, "Multi-dimensional imaging method and apparatus," U.S. Patent US 2007/0109177 A1, 17, 2007.

[2] "The internet of things — how the next evolution of the internet is changing everything," White Paper, Cisco, 2011.

[3] J. Rabaey, M. Ammer, J. da Silva, J.L., D. Patel, and S. Roundy, "Picoradio supports ad hoc ultra-low power wireless networking," *Computer*, vol. 33, no. 7, pp. 42–48, Jul 2000.

[4] J. Paradiso and T. Starner, "Energy scavenging for mobile and wireless electronics," *Pervasive Computing, IEEE*, vol. 4, no. 1, pp. 18–27, Jan.-March 2005.

[5] H. Yan, J. G. Macias-Montero, A. Akhnoukh, L. C. N. de Vreede, J. R. Long, and J. N. Burghartz, "An ultra-low-power BPSK receiver and demodulator based on injection-locked oscillators," *IEEE Trans. Microw. Theory Tech.*, vol. 59, pp. 1339–1348, May 2011.

[6] E. H. Armstrong, "Some recent developments of regenerative circuits," *Proceedings of the IRE*, vol. 10, Aug. 1922.

[7] B. Otis and J. Rabaey, *Ultra-Low Power Wireless Technologies for Sensor Networks*. New York: Springer, 2007.

[8] H. L. Thal, "New radiation Q limits for spherical wire antennas," *IEEE Trans. Antennas Propag.*, vol. 54, pp. 2757–2763, Oct. 2006.

[9] C. W. P. F *et al.*, "A 2.4GHz CMOS automatic matching network design for pacemaker applications," in *Circuits and Systems and TAISA Conference, 2009*, Jun. 2009, pp. 1–4.

[10] P. Sjoblom and H. Sjoland, "An adaptive impedance tuning CMOS circuit for ISM 2.4-GHz band," *Circuits and Systems I: Regular Papers, IEEE Transactions on*, vol. 52, no. 6, pp. 1115–1124, 2005.

[11] D. C. Daly, P. P. Mercier, M. Bhardwaj, A. L. Stone, Z. N. Aldworth, T. L. Daniel, J. Voldman, J. G. Hildebrand, and A. P. Chandrakasan, "A pulsed UWB receiver SoC for insect motion control," *IEEE J. Solid-State Circuits*, vol. 45, pp. 153–166, Jan. 2010.

[12] V. Pillai, H. Heinrich, D. Dieska, P. V. Nikitin, R. Martinez, and K. V. S. Rao, "An ultra-low-power long range battery/passive RFID tag for UHF and microwave bands with a current consumption of 700 nA at 1.5 V," *IEEE Trans. Circuits Syst. I*, vol. 54, pp. 1500–1512, Jul. 2007.

[13] P. Kolinko and L. Larson, "Passive RF receiver design for wireless sensor networks," in *IEEE/MTT-S International Microwave Symposium*, Jun. 3–8, 2007, pp. 567–570.

[14] A. Hennig and G. vom Bögel, "A data transmission technique for passive sensor-transponders in medicine," in *2010 IEEE International Conference on RFID*, Apr. 14–16, 2010, pp. 215–222.

[15] N. M. Pletcher, S. Gambini, and J. M. Rabaey, "A 52μW wake-up receiver with -72dBm sensitivity using an uncertain-IF architechture," *IEEE J. Solid-State Circuits*, vol. 44, pp. 269–280, Jan. 2009.

[16] A. Liscidini, A. Mazzanti, R. Tonietto, L. Vandi, P. Andreani, and R. Castello, "Single-stage low-power quadrature RF receiver front-end: The LMV cell," *IEEE J. Solid-State Circuits*, vol. 41, pp. 2832–2841, Dec. 2006.

[17] H.-H. Hsieh and L.-H. Lu, "Design of ultra-low-voltage RF frontends with complementary current-reused architectures," *IEEE Trans. Microw. Theory Tech.*, vol. 55, Jul. 2007.

[18] R. Malmqvist, M. Danestig, S. Rudner, and C. Svensson, "Theoretical analysis of sensitivity and Q-value for recursive active microwave integrated filters," *IEE Proc.-Microw. Antennas Propag.*, vol. 146, Aug. 1999.

[19] B. P. Otis and J. M. Rabaey, "A 300-μW 1.9-GHz CMOS oscillator utilizing micromachined resonators," *IEEE J. Solid-State Circuits*, vol. 38, Jul. 2003.

[20] N. M. Pletcher and J. M. Rabaey, "A 100μW, 1.9GHz oscillator with fully digital frequency tuning," in *Proceedings of ESSCIRC*, Grenoble, France, 2005, pp. 387–390.

[21] X. Duo, T. Torikka, L.-R. Zheng, M. Ismail, and H. Tenhunen, "On-chip versus off-chip passives in multi-band radio design," in *Electronics System-integration Technology Conference*, vol. 1, Dresden, 2006, pp. 221–232.

[22] J. Wight, J. Long, L. Carley, and T. Riley, "On-die synthesized inductors: Boon or bane?" *Microwave Magazine, IEEE*, vol. 11, no. 3, pp. 95–104, 2010.

[23] A. Wang, S.-H. Cho, C. G. Sodini, and A. P. Chandrakasan, "Energy-efficient modulation and MAC for asymmetric microsensor systems," in *Proceedings of ISLPED 2001*, Huntington Beach, CA, Aug. 2001.

[24] G. Chunlong, C. Zhong, and J. Rabaey, "Low power distributed MAC for ad hoc sensor radio networks," in *IEEE Global Telecommunications Conference*, vol. 5, Nov. 25–29, 2001, pp. 2944–2948.

[25] L. Gu and J. A. Stankovic, "Radio-triggered wake-up capability for sensor networks," in *10th IEEE Real-Time and Embedded Technology and Applications Symposium, RTAS 2004)*, May 25–28, 2004, pp. 27–36.

[26] S. Drago, F. Sebastiano, L. Breems, D. Leenaerts, K. Makinwa, and B. Nauta, "Impulse-based scheme for crystal-less ULP radios," *Circuits and Systems I: Regular Papers, IEEE Transactions on*, vol. 56, no. 5, pp. 1041 –1052, May 2009.

[27] R. Floyd, "RFID: Yesterday, today, and tomorrow," *Potentials, IEEE*, vol. 31, no. 6, pp. 11–46, 2012.

[28] J. Landt, "The history of RFID," *Potentials, IEEE*, vol. 24, no. 4, pp. 8–11, 2005.

[29] B. Nilsson, L. Bengtsson, B. Svensson, U. Bilstrup, and P.-A. Wiberg, "An active backscatter wake-up and tag identification extraction protocol for low cost and low power active RFID," in *RFID-Technology and Applications (RFID-TA), 2010 IEEE International Conference on*, Jun. 2010, pp. 86 – 91.

[30] J.-Y. Chen, M. P. Flynn, and J. P. Hayes, "A fully integrated auto-calibrated super-regenerative receiver in 0.13-μm CMOS," *IEEE J. Solid-State Circuits*, vol. 42, Sep. 2007.

[31] J. Ayers, K. Mayaram, and T. Fiez, "An ultralow-power receiver for wireless sensor networks," *Solid-State Circuits, IEEE Journal of*, vol. 45, no. 9, pp. 1759 –1769, Sep. 2010.

[32] E. Nilsson and C. Svensson, "Envelope detector sensitivity and blocking characteristics," in *Circuit Theory and Design (ECCTD), 2011 20th European Conference on*, Aug. 2011, pp. 773 –776.

[33] *IEEE Std 802.3-2008 (Revision of IEEE Std 802.3-2005).*

[34] X. Huang, S. Rampu, X. Wang, G. Dolmans, and H. de Groot, "A 2.4GHz/915MHz 51μW wake-up receiver with offset and noise suppression," in *IEEE International Solid-State Circuits Conference 2010*, Feb. 9, 2010, pp. 222–224.

[35] Auto-ID Center. (2002) 860MHz-930MHz class I radio frequency identification tag radio frequency and logical communication interface specification candidate recommendation, version 1.0.1. [Online]. Available: www.gs1.org/epcglobal/standards/specs

[36] S. Solda, M. Caruso, A. Bevilacqua, A. Gerosa, D. Vogrig, and A. Neviani, "A 5 Mb/s UWB-IR transceiver front-end for wireless sensor networks in 0.13 μm CMOS," *Solid-State Circuits, IEEE Journal of*, vol. 46, no. 7, pp. 1636 –1647, Jul. 2011.

[37] A. Gerosa, S. Solda, A. Bevilacqua, D. Vogrig, and A. Neviani, "An energy-detector for noncoherent impulse-radio UWB receivers," *Circuits and Systems I: Regular Papers, IEEE Transactions on*, vol. 56, no. 5, pp. 1030 –1040, May 2009.

[38] T. Orhaug and B. Höglund, *Rymdkommunikationsteknik*, 5th ed., Göteborg, 1974.

[39] C. Svensson and J. J. Wikner, "Power consumption of analog circuits: a tutorial," *Analog Integrated Circuits and Signal Processing*, vol. 65, Nov. 2010.

[40] J.-Y. Park, D.-W. Kim, Y.-S. Son, J.-C. Ha, J.-K. Song, C.-S. Jang, and W.-Y. Jung, "Low-capacitance low-voltage triggered SCR ESD clamp using nMOS with asymmetric drain for RF ICs," *Microwave Theory and Techniques, IEEE Transactions on*, vol. 59, no. 2, pp. 360–367, 2011.

[41] C. A. Balanis, *Antenna Theory*. hoboken: Wiley, 2005.

[42] B. Razavi, "A study of phase noise in CMOS oscillators," *Solid-State Circuits, IEEE Journal of*, vol. 31, no. 3, pp. 331–343, 1996.

[43] W. G. Carrara, R. S. Goodman, and R. M. Majewski, *Spotlight Synthetic Aperture Radar: Signal Processing Algorithms*. Norwood: Artech house, 1995.

[44] P. Dammert, "Accuracy of INSAR measurements in forested areas," in *FRINGE 96*, Zurich, Switzerland, Oct. 1996. [Online]. Available: http://www.geo.unizh.ch/rsl/fringe96/papers/dammert/

[45] C. T. Wang, H. T. Wang, D. C. Chern, N. Y. Chen, and L. S. Liang, "A study on differential interferometry in subsidence," in *Proceedings ACRS*, Taipei, Taiwan, Dec. 2000. [Online]. Available: http://www.gisdevelopment.net/aars/acrs/2000/ts14/sari0004.asp

[46] A. R. Thompson, J. M. Moran, and J. George W. Swenson, *Interferometry and Synthesis in Radio Astronomy*, 2nd ed. USA: John Wiley and Sons, 2001.

[47] J. Starck, E. Pantin, and F. Murtagh, "Deconvolution in astronomy: A review," *Astronomical Society of the Pacific*, pp. 1051–1069, Oct. 2002.

[48] T. Cornwell and K. Evans, "A simple maximum entropy deconvolution algorithm," *Astronomy and Astrophysics*, pp. 77–83, 1985.

[49] J. Hogbom, "Aperture synthesis with a non-regular distribution of interferometer baselines," *Astronomy and Astrophysics Supplement*, vol. 15, pp. 417–426, Jun. 1974.

[50] R. Bose, A. Freedman, and B. Steinberg, "Sequence CLEAN: a modified deconvolution technique for microwave images of contiguous targets," *IEEE Trans. Aerosp. Electron. Syst.*, vol. 38, pp. 89–97, Jan. 2002.

[51] E. Nilsson and L. B. Baath, "Radar interferometric measurements with a planar patch antenna array," *IEEE Sensors J.*, 2006.

[52] P.-S. Kildahl, *Foundation of Antennas*. Lund, Sweden: Studentlitteratur, 2000.

[53] F. T. Ulaby, R. K. Moore, and A. K. Fung, *Microwave Remote Sensing, Active and Passive*. Norwood, MA: Artech House, 2003.

[54] A. T. Moffet, "Minimum-redundancy linear arrays," *IEEE Trans. Antennas Propag.*, vol. 16, pp. 172–175, Mar. 1968.

[55] D. M. Pozar, *Microwave Engineering.* Amherst, MA: John Wiley and Sons, 1998.

[56] R. Garg, P. Bhartia, I. Bahl, and A. Ittipiboon, *Microstrip Antenna Design Handbook.* Norwood, USA: Artech House, 2001.

[57] F. Sebastiano, L. Breems, K. Makinwa, S. Drago, D. Leenaerts, and B. Nauta, "A low-voltage mobility-based frequency reference for crystal-less ULP radios," *Solid-State Circuits, IEEE Journal of*, vol. 44, no. 7, pp. 2002 –2009, july 2009.

[58] U. Denier, "Analysis and design of an ultralow-power CMOS relaxation oscillator," *Circuits and Systems I: Regular Papers, IEEE Transactions on*, vol. 57, no. 8, pp. 1973 –1982, Aug. 2010.

[59] J. Laskar, "CMOS, cognitive and mmW: A wireless revolution," in *Radio and Wireless Symposium (RWS), 2012 IEEE*, 2012, pp. 211–214.

[60] M. Tiebout, H. D. Wohlmuth, H. Knapp, R. Salerno, M. Druml, M. Rest, J. Kaeferboeck, J. Wuertele, S. Ahmed, A. Schiessl, R. Juenemann, and A. Zielska, "Low power wideband receiver and transmitter chipset for mm-wave imaging in SiGe bipolar technology," *Solid-State Circuits, IEEE Journal of*, vol. 47, no. 5, pp. 1175–1184, 2012.

[61] J. Rabaey, "The swarm at the edge of the cloud - a new perspective on wireless," in *VLSI Circuits (VLSIC), 2011 Symposium on*, 2011, pp. 6–8.

[62] T. Burd, T. Pering, A. Stratakos, and R. Brodersen, "A dynamic voltage scaled microprocessor system," *Solid-State Circuits, IEEE Journal of*, vol. 35, no. 11, pp. 1571–1580, 2000.

[63] M. Trotter and G. Durgin, "Survey of range improvement of commercial RFID tags with power optimized waveforms," in *RFID, 2010 IEEE International Conference on*, Apr. 2010, pp. 195 –202.

[64] E. Lind and L.-E. Wernersson, "Design of RF properties for vertical nanowire MOSFETs," *Nanotechnology, IEEE Transactions on*, vol. 10, no. 4, pp. 668–673, 2011.